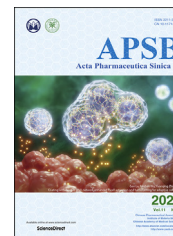




Chinese Pharmaceutical Association  
Institute of Materia Medica, Chinese Academy of Medical Sciences

Acta Pharmaceutica Sinica B

[www.elsevier.com/locate/apsb](http://www.elsevier.com/locate/apsb)  
[www.sciencedirect.com](http://www.sciencedirect.com)



ORIGINAL ARTICLE

# Discovery of 4-arylthiophene-3-carboxylic acid as inhibitor of ANO1 and its effect as analgesic agent



Yuxi Wang<sup>a,†</sup>, Jian Gao<sup>a,†</sup>, Song Zhao<sup>b</sup>, Yan Song<sup>a</sup>, Han Huang<sup>a</sup>,  
Guiwang Zhu<sup>a</sup>, Peili Jiao<sup>a</sup>, Xiangqing Xu<sup>b</sup>, Guisen Zhang<sup>c</sup>,  
Kewei Wang<sup>d,\*</sup>, Liangren Zhang<sup>a,\*</sup>, Zhenming Liu<sup>a,\*</sup>

<sup>a</sup>State Key Laboratory of Natural and Biomimetic Drugs, School of Pharmaceutical Sciences, Peking University, Beijing 100191, China

<sup>b</sup>Jiangsu Nhwa Pharmaceutical Co., Ltd., Xuzhou 221116, China

<sup>c</sup>College of Life Science and Technology, Jiangsu Ocean University, Lianyungang 222005, China

<sup>d</sup>Department of Pharmacology, School of Pharmacy, Qingdao University, Qingdao 266021, China

Received 13 September 2020; received in revised form 26 October 2020; accepted 4 November 2020

## KEY WORDS

ANO1 (anoctamin 1,  
TMEM16A);  
Inhibitor;  
Synthesis;  
Structure–activity  
relationship;  
Analgesia

**Abstract** Anoctamin 1 (ANO1) is a kind of calcium-activated chloride channel involved in nerve depolarization. ANO1 inhibitors display significant analgesic activity by the local peripheral and intrathecal administration. In this study, several thiophenecarboxylic acid and benzoic acid derivatives were identified as novel ANO1 inhibitors through the shape-based virtual screening, among which the 4-arylthiophene-3-carboxylic acid analogues with the best ANO1 inhibitory activity were designed, synthesized and compound **42** ( $IC_{50} = 0.79 \mu\text{mol/L}$ ) was finally obtained. Compound **42** selectively inhibited ANO1 without affecting ANO2 and intracellular  $\text{Ca}^{2+}$  concentration. Subsequently, the analgesic effect was investigated by intragastric administration in pain models. Compound **42** significantly attenuated allodynia which was induced by formalin and chronic constriction injury. Through homology modeling and molecular dynamics, the binding site was predicted to be located near the calcium-binding region between  $\alpha 6$  and  $\alpha 8$ . Our study validates ANO1 inhibitors having a significant analgesic effect by intragastric administration and also provides selective molecular tools for ANO1-related research.

© 2021 Chinese Pharmaceutical Association and Institute of Materia Medica, Chinese Academy of Medical Sciences. Production and hosting by Elsevier B.V. This is an open access article under the CC BY-NC-ND license (<http://creativecommons.org/licenses/by-nc-nd/4.0/>).

\*Corresponding authors. Tel: +86 532 82991070 (Kewei Wang), +86 10 82802567 (Liangren Zhang), +86 10 82805281 (Zhenming Liu).

E-mail addresses: [wangkw@qdu.edu.cn](mailto:wangkw@qdu.edu.cn) (Kewei Wang), [liangren@bjmu.edu.cn](mailto:liangren@bjmu.edu.cn) (Liangren Zhang), [zmliu@bjmu.edu.cn](mailto:zmliu@bjmu.edu.cn) (Zhenming Liu).

<sup>†</sup>These authors made equal contributions to this work.

Peer review under responsibility of Chinese Pharmaceutical Association and Institute of Materia Medica, Chinese Academy of Medical Sciences.

## 1. Introduction

Anoctamin 1 (ANO1, TMEM16A) is a kind of the calcium-activated chloride channel (CaCC) on cytomembrane, controlled by intracellular  $\text{Ca}^{2+}$  concentration and membrane potential<sup>1–8</sup>. ANO1 is mainly expressed in airway<sup>9,10</sup>, peripheral nervous system<sup>11</sup>, gastrointestinal smooth muscle<sup>12</sup>, and some tumors<sup>13–15</sup>, which mediates and controls anion permeation to fulfill airway and exocrine gland secretion, neuronal signal transduction, and rhythmic movements of the gastrointestinal system.

In the peripheral nervous system, ANO1 is distributed in nociceptors, dorsal root ganglia (DRG), and spinal nerves, involved in nerve depolarization<sup>11,16,17</sup>. ANO1 is capable of augmenting the excitability of DRG neurons under inflammatory or neuropathic conditions and thereby aggravates inflammation- or tissue injury-induced pathological pain<sup>18,19</sup>. Knockout or inhibition of ANO1 causes significant analgesic effects. Intrathecal injection of the ANO1 inhibitor reverts the spinal nerve ligation-induced mechanical allodynia in a dose-dependent manner<sup>16</sup>. The non-selective and selective CaCC blockers reduce formalin-induced flinching behavior mainly during phase 2 of the formalin test<sup>20</sup>.

ANO1 is considered as associated with inflammation-related pain caused by the changes in temperature, ion concentration in inflamed tissues, and inflammatory factors<sup>21</sup>. The elevated temperature of inflamed tissue activates temperature-sensitive calcium channels (such as transient receptor potential channel V1, TRPV1), which activates ANO1 not only by direct interaction<sup>21,22</sup> but also indirectly by increasing intracellular calcium ion concentrations<sup>23</sup>. Interleukin-4, an inflammatory factor in inflamed tissues or injured nerves, can promote the overexpression of ANO1, which may be related to allodynia<sup>5,16</sup>.

In the last 10 years, many ANO1 inhibitors (Fig. 1) are identified and synthesized including  $\text{CaCC}_{\text{inh}}\text{-A01}$  (1),  $\text{T16A}_{\text{inh}}\text{-A01}$  (2), MONNA (3), AACT (4), Ani9 (5), and digallic acid (6). More recently, some clinically used drugs and natural products are found to inhibit ANO1, such as niclosamide, nitazoxanide<sup>12</sup>, flavonoids<sup>29,30</sup>, resveratrol<sup>31</sup>, etc. Among these compounds, AACT<sup>10</sup> and Ani9<sup>27</sup> have ANO1/ANO2 selectivity (ANO2 is a homologous protein of ANO1 that functions as a CaCC in brain)<sup>32</sup>. These inhibitors were used in various pharmacodynamics studies: AACT suppresses isometric smooth muscle contraction in mouse ileum tissue<sup>10</sup>.  $\text{CaCC}_{\text{inh}}\text{-A01}$  and Ani9 inhibit the proliferation of ANO1 over-expressed tumor<sup>15,27</sup>. Niclosamide fully bronchodilates airways *in vitro*<sup>12</sup>.  $\text{CaCC}_{\text{inh}}\text{-A01}$ ,  $\text{T16A}_{\text{inh}}\text{-A01}$ , and MONNA attenuate formalin-induced hyperalgesia and allodynia by local peripheral and intrathecal administration<sup>16,19,20</sup>. In short, though

many ANO1 inhibitors have been found, their physiological functions are varied and not fully investigated. For the discovery of potential clinical application, the biological behaviors of ANO1 and its inhibitors need to be clearly elucidated, and more importantly, structurally diverse and active inhibitors are required.

In this study, to explore new ANO1 inhibitors and potential analgesic agents, we firstly performed a scaffold virtual screening starting from the 2-arylamidothiophene skeleton shared in  $\text{CaCC}_{\text{inh}}\text{-A01}$  (1) and AACT (4), and a series of thiophenic acid and benzoic acid derivatives showed ANO1 inhibition. Subsequently, the 4-arylthiophene-3-acid selected from the screening results was used as the starting hit for optimization. The inhibitory activities were evaluated by whole-cell patch clamp on ANO1-overexpressing Fischer rat thyroid (FRT) cells. The activity preferred compound was used for analgesic evaluation in various animal pain models. The finding of this study is helpful for the understanding of the structure–activity relationships (SARs) of ANO1 inhibitors and provides a selective inhibitor for probing the biological function of the ANO1 channel.

## 2. Results and discussions

### 2.1. Shape and electrostatic similarity-based virtual screening

The shape and electrostatic similarity-based virtual screening query were generated from the optimized conformation of  $\text{CaCC}_{\text{inh}}\text{-A01}$  in OPENEYE software (Fig. 2). 300,000 compounds from the SPECS chemical library and Chinese National Compound Library of Peking University (PKU\_CNCL) were screened followed by artificial selection of the molecules with Shape Tanimoto and EON index greater than 0.6. Seventy-six compounds, including thiophenic acid derivatives (Table 1, compounds 7–32), benzoic acid derivatives (Supporting Information Fig. S1, compounds S1–S13), and 37 other scaffold compounds (Fig. S1, compounds S14–S50). Their ANO1 inhibitory effects were tested using whole cell patch clamp at 100  $\mu\text{mol/L}$  in ANO1-overexpression FRT cell line.

Of these 76 structurally diversified compounds, we focused on three thiophene containing scaffolds (scaffolds 1–3) which  $\text{CaCC}_{\text{inh}}\text{-A01}$  and AACT share (compounds 7–32, Table 1), while the ANO1 inhibitory activity of other compounds was shown in Supporting Information Table S1 due to they showed relatively low ANO1 inhibitory activity in whole-cell patch clamp.

The scaffold 1 varies in the ring size of tetrahydrobenzo[*b*]thiophene in  $\text{CaCC}_{\text{inh}}\text{-A01}$  (1). Active compounds appeared to have *t*-butyl substitution as  $\text{R}_2$  (1 and 7). Compounds with 2-F-phenyl (10), 4-I-phenyl (12), and 1-naphthalene (14) as  $\text{R}_1$  were more active than others. Extending the amide linker by the double

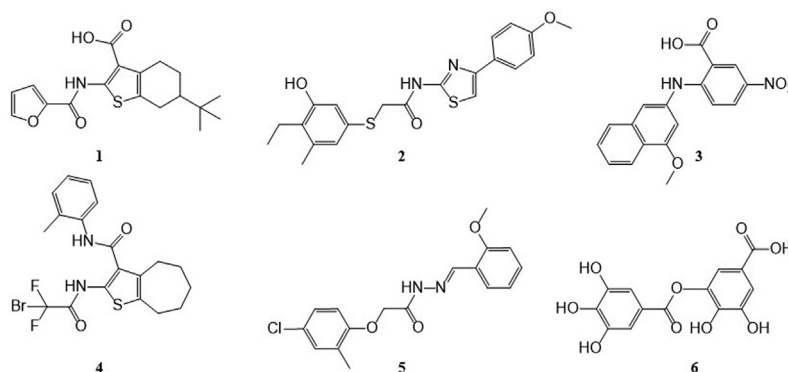


**Figure 1** Chemical structure of reported ANO1 inhibitors.

bond (**15**) or methylene (**16**) is detrimental to the ANO1 inhibitory activity. Expanding the thiophene-fused aliphatic ring contributes to the enhancement of ANO1 inhibitory activity, for example, compound **17** ( $n = 3$ ) is better than compound **9** ( $n = 2$ ).

In scaffold 2, the moiety of tetrahydrobenzothiophene is replaced by thiophene in which positions 4' and 5' are substituted by alkyl or aromatic groups. Compounds **22** and **23** display comparative ANO1 inhibitory activity with CaCC<sub>inh</sub>-A01 (**1**), indicating the feasibility of breaking tetrahydrobenzo-ring. Alkyl substitution at R<sub>2</sub> (**22** and **23**) is more favorable than non-substitution (**21**). Among the substituents of the R<sub>1</sub>, 4-methylphenyl (**22**) is superior to 4-*tert*-butylphenyl (**24**) and 3-bromophenyl (**25**). Extending the amide linker by the double bond is unfavorable to the ANO1 inhibitory activity.

Scaffold 3 replaces the R<sub>2</sub> position in scaffold 2 with an aromatic group. Compound **28** with 4-(4-oxymethylbenzo)-thiophene scaffold has higher ANO1 inhibitory activity than CaCC<sub>inh</sub>-A01 (**1**). The 4-*tert*-butylphenyl substituent of R<sub>1</sub> (**28**) is more active than 2-methoxyphenyl (**27**). Additionally, if the carboxyl group of R<sub>3</sub> is replaced by an ester group, the ANO1 inhibitory activity declined (**29–32**).

Based on the preliminary SAR analysis, compound **28** with 4-arylthiophene-3-carboxylic acid backbone was selected as a hit for further optimization.

## 2.2. Synthesis and optimization of 4-arylthiophene-3-carboxylic acid derivatives

Based on compound **28**, further optimization strategies involved three steps: firstly, 4-methoxyphenyl at thiophene 4' position was

replaced by various substituted phenyl and naphthyl groups. Then, the substructure on the carbonyl side of the amide was replaced by the preferred groups from the above virtual screening process. Finally, combined the substructures of tetrahydrobenzothiophene in CaCC<sub>inh</sub>-A01 and the aryl substituted thiophene at 4' position in compound **28** to expand the volume of thiophene containing scaffold. ANO1 inhibitory rate was conducted by yellow fluorescence protein (YFP) fluorescence quenching assay<sup>24</sup> in ANO1-overexpressing FRT cell line and was calculate by Eq. (1):

$$\text{Inhibition rate (\%)} = (K_{\text{cont}} - K_{\text{comp}})/K_{\text{cont}} \times 100 \quad (1)$$

where  $K_{\text{cont}}$  means the slope of negative control,  $K_{\text{comp}}$  means the slope of the test compound. The ANO1 inhibitory IC<sub>50</sub> was determined based on the inhibitory rate in 7 compound concentrations.

Compound **42** and its derivatives were synthesized by three steps (Schemes 1 and 2). Firstly, ketones reacted with cyanoacetate and sulfur to form 2-aminothiophene-3-carboxylate acid ethyl ester intermediates by the Gewald reaction<sup>33</sup>. Then these intermediates are coupled with acyl chloride to form the amides derivatives. Finally, the hydrolysis reactions were conducted to form final products.

## 2.3. SAR analysis of 4-arylthiophene-3-carboxylic acid derivatives

For the substituents at the R<sub>1</sub> position (Table 2), most of the substituents are acceptable except for 4-CF<sub>3</sub>-phenyl (**35**) and 2,4-dichloridephenyl substitutions (**38**). The most potent 4-

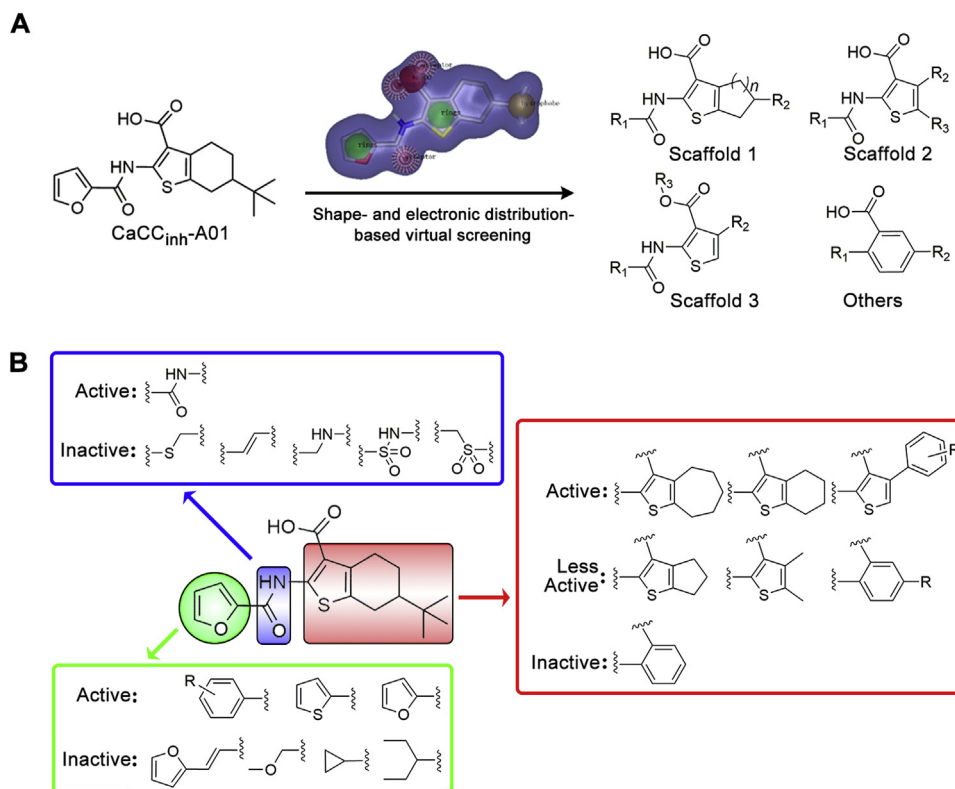


**Figure 2** Shape and electronic similarity-based virtual screening. (A) Scaffolds obtained from shape-based virtual screening; the purple surface represents the virtual screening query in OPENEYE software. (B) The general structure–activity relationships which produced by virtual screening.

**Table 1** Structure and ANO1 inhibitory activity of thiophenic acid derivatives.

Compd.	<i>n</i>	Structure			Inh. (%) <sup>a</sup>
		R <sub>1</sub>	R <sub>2</sub>	R <sub>3</sub>	
<div style="display: flex; justify-content: space-around; align-items: flex-start;"> <div style="text-align: center;"> <p>Scaffold 1</p> <p>7–20</p> </div> <div style="text-align: center;"> <p>Scaffold 2</p> <p>21–26</p> </div> <div style="text-align: center;"> <p>Scaffold 3</p> <p>27–32</p> </div> </div>					
Compd.	<i>n</i>	R <sub>1</sub>	R <sub>2</sub>	R <sub>3</sub>	Inh. (%) <sup>a</sup>
1	2		<i>t</i> -Bu	–	78.3
7	2		<i>t</i> -Bu	–	82.8
8	2		–CH <sub>3</sub>	–	25.4
9	2		–H	–	37.8
10	2		–H	–	74.3
11	2		–H	–	51.6
12	2		–H	–	69.3
13	2		–H	–	30.3
14	2		–H	–	72.5
15	2		–H	–	45.8
16	2		–H	–	18.3
17	3		–H	–	70.5
18	3		–H	–	45.9
19	3		–H	–	80.6
20	1		–H	–	35.1
21	–		–H	–CH <sub>3</sub>	33.1
22	–		–CH <sub>3</sub>	–CH <sub>3</sub>	84.4
23	–		–CH <sub>3</sub>	–CH <sub>2</sub> CH <sub>2</sub> CH <sub>3</sub>	74.9
24	–		–CH <sub>3</sub>	–CH <sub>3</sub>	35.8
25	–		–CH <sub>3</sub>	–CH <sub>3</sub>	42.5
26	–		–CH <sub>3</sub>	–CH <sub>3</sub>	19.6
27	–			–H	33.4
28	–			–H	89.2
29	–			–CH <sub>3</sub>	12.4

Table 1 (continued)

30	—			—C <sub>2</sub> H <sub>5</sub>	21.4
31	—			—CH <sub>3</sub>	46.1
32	—			—CH <sub>3</sub>	13.0

<sup>a</sup>ANO1 inhibition rate of compounds at 100 μmol/L was determined using whole-cell patch clamp on ANO1-overexpressing FRT cells at +100 mV voltage. Data are represented by mean ± SEM, n = 5.

chlorophenyl (**34**) was selected for R<sub>2</sub> optimization. For this, we selected the preferred fragments which showed in the previous virtual screening (such as thiophenyl, 1-naphthyl, and 4-*t*-butylphenyl). Among which 1-naphthyl (**42**) substituted compound showed the highest ANO1 inhibitory activity (IC<sub>50</sub> = 0.79 μmol/L). Besides, the inhibitory activity of ANO1 was slightly decreased when 2-thiophenyl (**40**) and 4-methyl-1-naphthyl (**46**) were substituted. In summary, when R<sub>1</sub> was substituted with 4-Cl-phenyl and R<sub>2</sub> with 1-naphthyl, the compound showed the strongest ANO1 inhibitory activity (compound **42**).

Compounds **47–53** combined the substructures of tetrahydrobenzothiothiophene in CaCC<sub>inh</sub>-A01 and the aryl substituted thiophene at 4' position in scaffold 3 (Table 3). When the R<sub>1</sub> was H (**47**), the inhibitory activity against ANO1 was higher than that of the methoxy group (**48**). Methyl substitution at R<sub>2</sub> and R<sub>3</sub> positions (**42**) favored ANO1 inhibitory activity. 1-Naphthyl (**51**) or 2-naphthyl (**50**) at R<sub>4</sub> position was beneficial to ANO1 inhibition. Compound **53** was more active than compound **47**, showed that the thiophene-fused a larger cycloalkane had a higher ANO1 inhibitory activity. It indicated that the flexibility between thiophene and benzene rings might favor activity. However, compounds **47–53** showed poor solubility in synthesis (only completely soluble in DMSO, slightly soluble in methanol, insoluble in water and DCM), which would cause a lot of trouble for further study, so we terminated the optimization of these scaffolds.

Based on the SAR studies of thiophene-containing ANO1 inhibitors (both in virtual screening and structure optimization), compound **42** (IC<sub>50</sub> = 0.79 μmol/L) was finally selected for further pharmacokinetic and pharmacodynamics study.

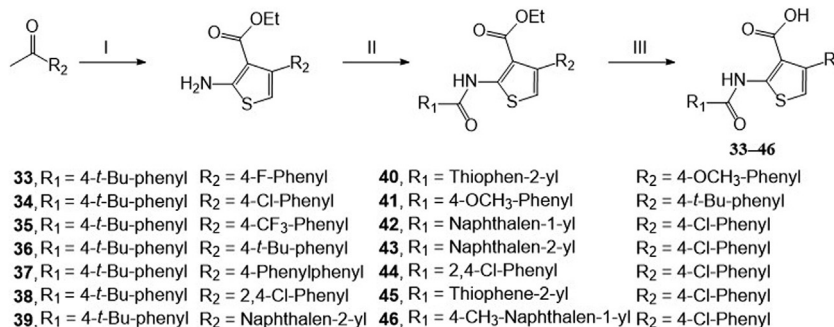
#### 2.4. Electrophysiology and Ca<sup>2+</sup> fluorescence investigations of compound **42**

To verify the inhibitory activity of compound **42** on ANO1, we performed whole-cell patch clamp in ANO1-overexpressing FRT cells as previously described<sup>10</sup>. In this experiment, the ANO1 channel was activated by 1 μmol/L intracellular Ca<sup>2+</sup> followed by changing the membrane potential +100 to −100 mV and comparing the evoked CaCC current before and after treatment. As shown in Fig. 3A, 30 μmol/L compound **42** significantly suppressed the CaCC current and was more potent than Ani9.

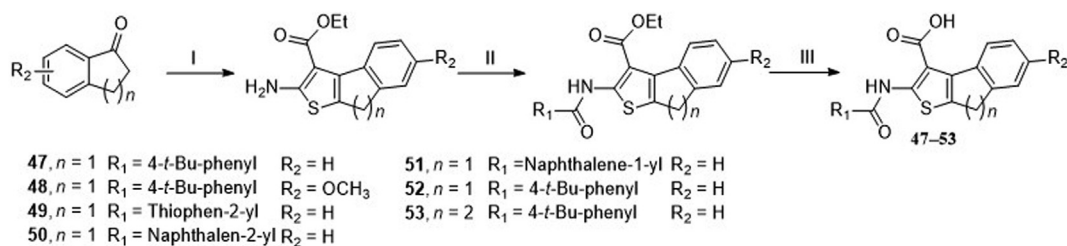
ANO1 is activated by intracellular Ca<sup>2+</sup>, and if the compound inhibits the Ca<sup>2+</sup> transmembrane, it will aggravate its ANO1 inhibitory effect. Calcium fluorescent dye Cal520<sup>TM</sup> was used to evaluate the influence of compound **42** on intracellular Ca<sup>2+</sup> concentration. Amlodipine was selected as a positive control. After 2 h pretreatment with Cal520<sup>TM</sup>, compound **42** and ATP were added in turn to evoke the Ca<sup>2+</sup> influx across cytomembrane, which showed the maximum relative fluorescence units (RFU) of the control group increased to 2.3 folds of the initial value and the RFU of amlodipine remained unchanged (Fig. 3B and C). Compound **42** almost did not affect Ca<sup>2+</sup> influx (1.9 folds than initial value), and CaCC<sub>inh</sub>-A01 slightly suppressed Ca<sup>2+</sup> influx (1.5 folds than initial value), whereas Ani9 hinders Ca<sup>2+</sup> transmembrane.

#### 2.5. ANO1/ANO2 channels selectivity of compound **42**

ANO2 coexists with BK (large conductance calcium-activated potassium) and SK (small conductance calcium-activated potassium) channels in inferior olivary neurons that participate in the



**Scheme 1** Synthetic route of 4-arylthiophene-3-carboxylic acid derivatives. Reagents and conditions: (I) step 1: ethyl cyanoacetate, morpholine, acetic acid, ethanol, 60 °C, 3 h, argon; step 2: sulfur, argon, 60 °C, 36–48 h. (II) Aryl substituted acid chloride, TEA, DCM, rt, 8 h. (III) NaOH, H<sub>2</sub>O, MeOH, THF, 60 °C, 8 h.



**Scheme 2** Synthetic route of 8*H*-indeno [2,1-*b*] thiophene-3-carboxylic acid and 4, 5-dihydronaphtho [2,1-*b*] thiophene-1-carboxylic acid derivatives. Reagents and conditions: (I) step 1: ethyl cyanoacetate, ammonium acetate, toluene, acetic acid, reflux, 12 h, argon; step 2: sulfur, ethanol, argon, 60 °C, 36–48 h. (II) Aryl substituted acid chloride, TEA, DCM, rt, 8 h. (III) NaOH, H<sub>2</sub>O, MeOH, THF, 60 °C, 8 h.

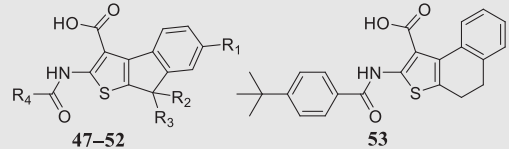
control of motor learning and timing<sup>34</sup>. ANO1-targeting analgesics lacking ANO1/ANO2 selectivity may cause potential central nervous system adverse effects. Thus, the ANO1/ANO2 selectivity of compound **42** was evaluated. ANO2 gene was transiently transfected into HEK293 cell, and then ANO2-mediated CaCC

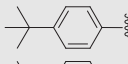
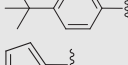
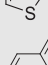
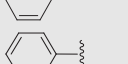
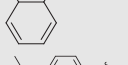
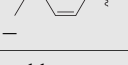
current was recorded by whole-cell patch clamp. The detailed method is the same as the reference<sup>35</sup>. The ANO1 and ANO2 pan-inhibitor CaCC<sub>inh</sub>-A01 was used as a negative control, and ANO1 selective inhibitor Ani9 was applied to be a positive control. The results showed that compound **42** at 30 μmol/L had little effect on

**Table 2** Structure and ANO1 inhibitory IC<sub>50</sub> of 4-arylthiophene-3-carboxylic acid derivatives.

Compd.	R <sub>1</sub>	R <sub>2</sub>	IC <sub>50</sub> (μmol/L) <sup>a</sup>
<b>1</b>	—	—	2.1
<b>28</b>			6.38
<b>33</b>			9.62
<b>34</b>			1.34
<b>35</b>			>100
<b>36</b>			3.67
<b>37</b>			2.30
<b>38</b>			>100
<b>39</b>			1.29
<b>40</b>			25.51
<b>41</b>			2.28
<b>42</b>			0.79
<b>43</b>			2.45
<b>44</b>			1.24
<b>45</b>			1.74
<b>46</b>			14.50

<sup>a</sup>IC<sub>50</sub> value was determined by YFP fluorescence quenching assay. Data are represented by mean ± SEM,  $n = 3$ .

**Table 3** Structure and ANO1 inhibitory IC<sub>50</sub> of compounds **47–53**.


Compd.	R <sub>1</sub>	R <sub>2</sub>	R <sub>3</sub>	R <sub>4</sub>	IC <sub>50</sub> (μmol/L) <sup>a</sup>
<b>1</b>	—	—	—	—	2.1
<b>47</b>	H	H	H		12.59
<b>48</b>	OCH <sub>3</sub>	H	H		28.94
<b>49</b>	H	H	H		11.29
<b>50</b>	H	H	H		1.91
<b>51</b>	H	H	H		2.21
<b>52</b>	H	CH <sub>3</sub>	CH <sub>3</sub>		3.33
<b>53</b>	—	—	—	—	5.15

IC<sub>50</sub> value was determined by YFP fluorescence quenching assay. Data are represented by mean ± SEM, *n* = 3.

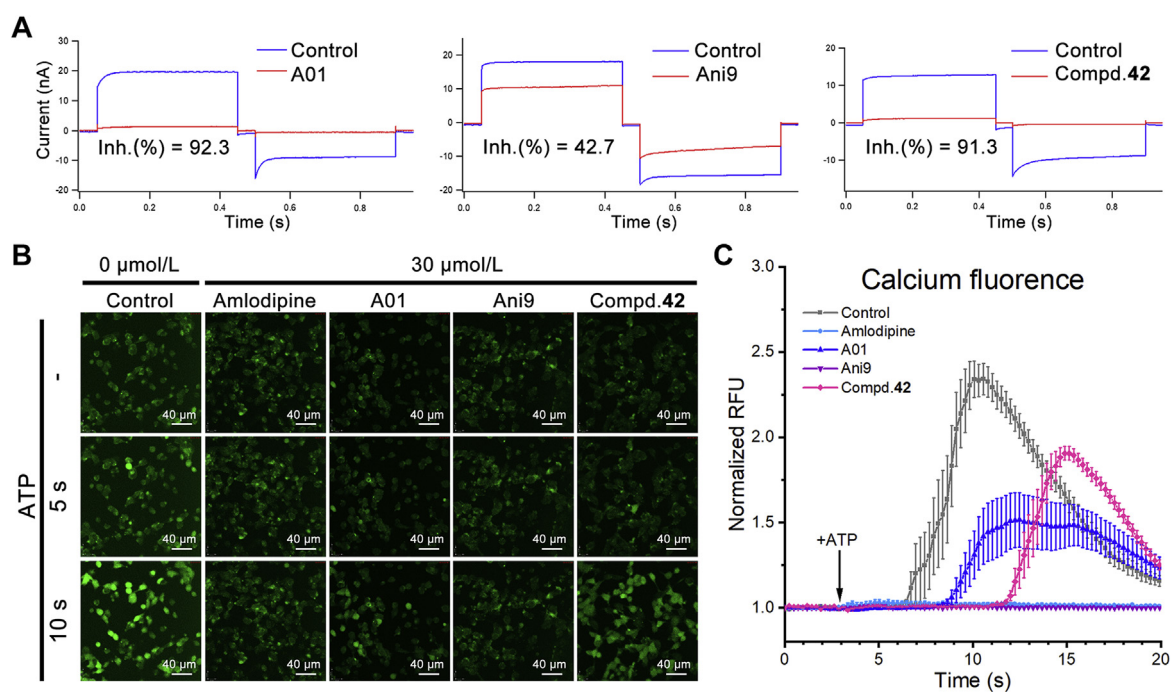


**Figure 3** ANO1 inhibitory activity validation. (A) CaCC current in whole-cell patch-clamp; FRT cells were clamped from the holding potential of 0 mV for 50 ms to 100 mV for 400 ms and then repolarized to  $-100$  mV for 400 ms and subsequently returned to 0 mV. Current curve is representative of similar results obtained in two independent experiments per compound and was repeat tested more than 5 times in each independent experiment; the inhibitory rate (Inh. %) was calculated from the current under  $+100$  mV potential; data are represented by mean ± SEM, *n* = 2; the concentration of compound is  $30$  μmol/L. (B) Ca<sup>2+</sup> fluorescence induced by  $200$  μmol/L ATP under  $30$  μmol/L compounds concentration treated; green point derived from calcium fluorescent dye Cal 520<sup>TM</sup>; scale bar,  $40$  μmol/L; images are representative of similar results obtained in three independent experiments per compound. (C) Quantification of Ca<sup>2+</sup> fluorescence in 20 s; results represent mean ± SEM for the 8 of independent fields ( $20$  μm ×  $20$  μm) per compound shown in (B).

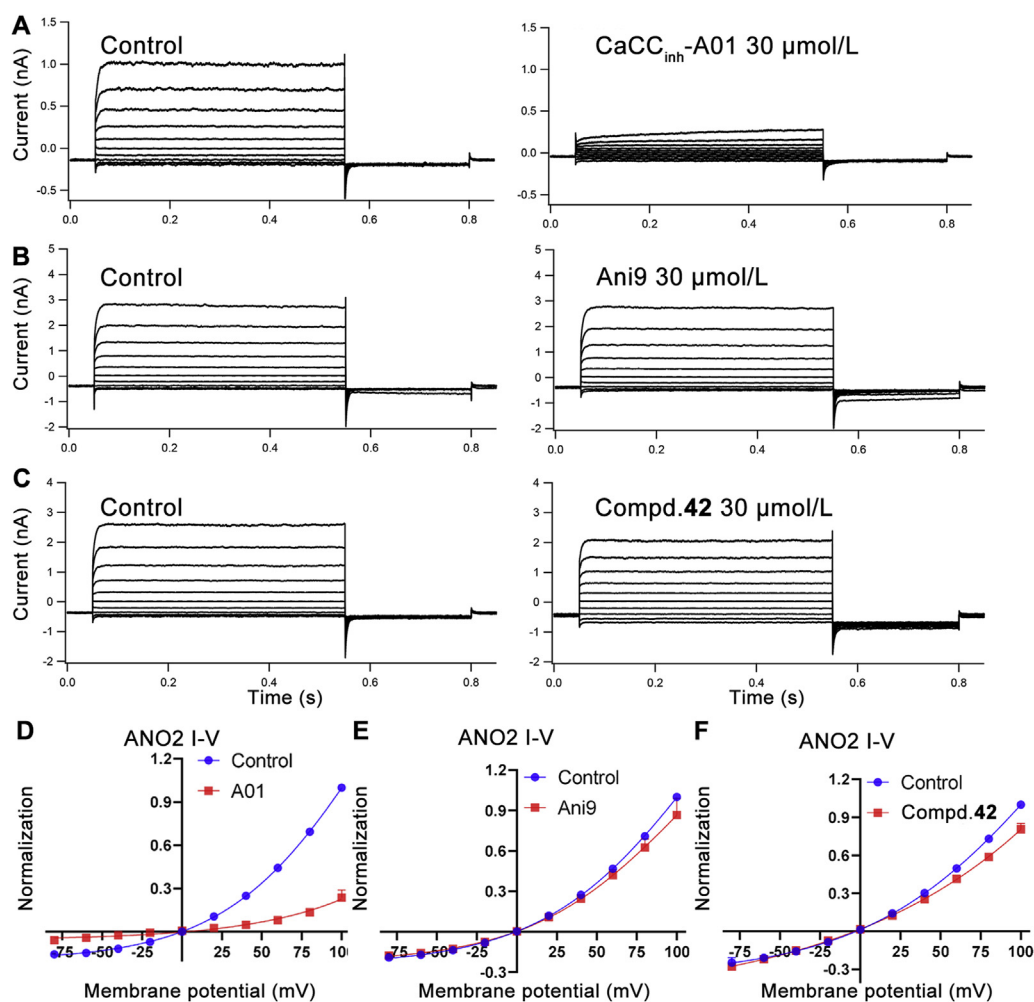


**Figure 4** Compound **42** performs little effect on ANO2 induced CaCC current at 30 μmol/L. (A), (B) and (C): representative traces of ANO2 currents at pCa<sup>2+</sup> 6.0 in the pipette solution from HEK293 cells expressing ANO2; currents were recorded under control conditions and after application by 30 μmol/L compounds. HEK293 cells were depolarized from the holding potential of -40 mV to test potentials (+100 to -80 mV) by +20 mV increment for 500 ms and subsequently repolarized to -80 mV for 250 ms every 15 s; current curve is representative of similar results obtained in two independent experiments per compound and was repeat tested more than 5 times in each independent experiment. (D), (E) and (F): current-voltage relationships from the experiment showed in (A), (B) and (C); data are represented by mean ± SEM, *n* = 10; current values were measured at the end of each voltage step.

ANO2 induced CaCC current. The ANO1/ANO2 selectivity of compound **42** is slightly weaker than that of Ani9 but much higher than that of CaCC<sub>inh</sub>-A01 (Fig. 4).

## 2.6. Stability and MDCK permeability of compound **42**

We wanted to test the *in vivo* analgesic activity of ANO1 inhibitors by intragastric gavage (i.g.) administration rather than local peripheral and intrathecal administration as previously

reported<sup>16,19,20</sup>, so compound **42** was evaluated for acid-base stability and intestinal absorbability to ensure it could be absorbed by animals.

### 2.6.1. Stability of compound **42** under different pH condition

The acid-base stability of compounds was tested under different pH buffer incubation by HPLC, which showed compound **42** remained stable in both acidic and alkaline environments (Table 4).

**Table 4** Compound stability under different pH conditions.

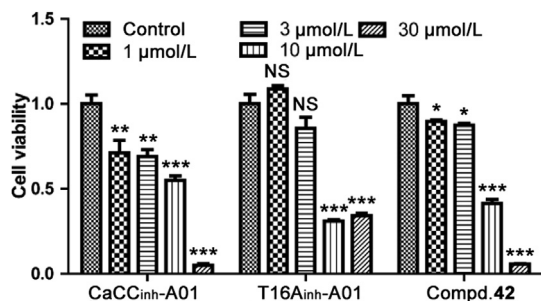
Compd.	5 h residual compound under different pH (%) <sup>a</sup>				
	pH 1.0	pH 4.0	pH 6.8	pH 7.4	pH 9.0
CaCC <sub>inh</sub> -A01	93.8 ± 4.0	85.3 ± 8.1	94.9 ± 2.9	98.7 ± 0.7	97.6 ± 1.2
<b>42</b>	99.0 ± 4.6	99.4 ± 4.4	99.2 ± 4.9	99.4 ± 3.5	99.5 ± 0.9

<sup>a</sup>Data are represented by the mean ± SD, *n* = 3.



**Table 5** MDCK permeability of compound **42**.

Compd.	$P_{app}$ (cm/s) <sup>a</sup>	$F$ prediction (%) <sup>b</sup>
CaCC <sub>inh</sub> -A01	$1.73 \times 10^{-5}$	>70
<b>42</b>	$1.38 \times 10^{-5}$	>70

<sup>a</sup> $P_{app}$ , permeability apparent coefficient.<sup>b</sup> $F$  prediction, oral bioavailability prediction; data are represented by mean  $\pm$  SD,  $n = 3$ .**Figure 5** Proliferation of CHO cells incubated with ANO1 inhibitors. Bar graph represents cytotoxicity of ANO1 inhibitors on CHO cell proliferation;  $n = 3$ ; data are represented by mean  $\pm$  SEM; NS, no significant, \* $P < 0.05$ , \*\* $P < 0.01$ , \*\*\* $P < 0.001$  compared to the 0.1% (v/v) DMSO in each group (control),  $t$ -test.

### 2.6.2. MDCK permeability of compound **42**

We performed the trans-well assay in the Madin–Darby canine kidney (MDCK) cell line to simulate compound absorption in the small intestine. Both compound **42** and CaCC<sub>inh</sub>-A01 passed through MDCK cells, indicating all of the two compounds could be absorbed by intestinal cells (Table 5).

### 2.7. Cytotoxicity and acute toxicity of compound **42**

#### 2.7.1. Proliferative cytotoxicity of compound **42**

Sulforhodamine B (SRB) assay in Chinese Hamster Ovary (CHO) cells was conducted to examine the proliferative cytotoxicity of

compound **42** incubated for 72 h (Fig. 5). All of the testing ANO1 inhibitors displayed proliferation inhibitory activity at 10  $\mu$ mol/L or higher. Compound **42** and T16A<sub>inh</sub>-A01 had a weak effect on proliferation under 1 and 3  $\mu$ mol/L, while CaCC<sub>inh</sub>-A01 inhibited cell proliferation at all concentrations tested.

#### 2.7.2. Acute toxicity of compound **42**

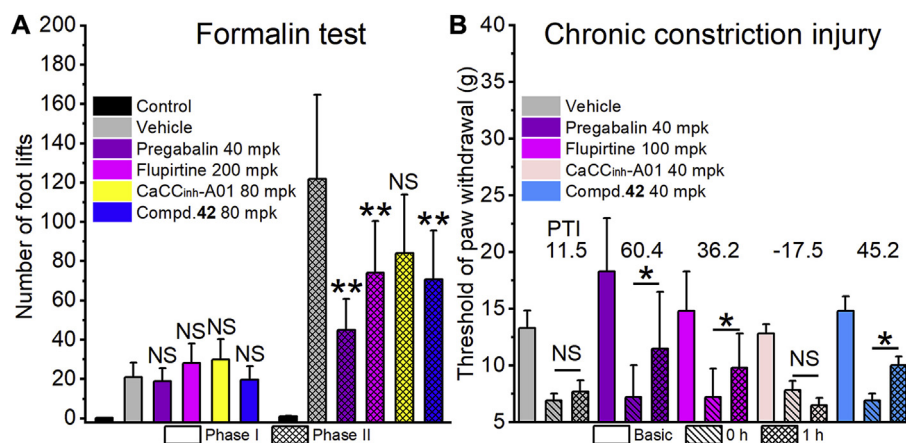
The acute toxicity was carried out in 6–8 weeks aged C57BL/6 male mice which were treated with 1000 mg/kg compound **42** by i.g. administration. All mice survived and no intense acute toxic response (such as coma, tachypnea, and moribund status) was observed in 72 h. The acute toxicity test showed that compound **42** is safe at the dose of 1000 mg/kg or lower by i.g. administration.

### 2.8. In vivo analgesic effects of compound **42**

The preliminary *in vivo* analgesic effects of compound **42** were investigated in the formalin test (Fig. 6A), chronic constriction injury model (Fig. 6B), hot plate test (Supporting Information Fig. S3) and writhing test (Supporting Information Fig. S4).

In the formalin test, phase 1 of the nociceptive response began immediately after formalin administration and then declined gradually in approximately 10 min. Phase 2 began about 15 min after formalin administration and lasted about 1 h. Pregabalin and flupirtine were selected as positive compounds. The results showed that these compounds had no significant effect on the number of foot lifts compared with the vehicle group (Fig. 6A). While, it was very encouraging that 80 mg/kg compound **42** (70 foot lifts) showed a significant analgesic effect in phase 2 compared with vehicle (121 foot lifts), which was almost as effective as flupirtine at 200 mg/kg (74 foot lifts) and pregabalin at 40 mg/kg (44 foot lifts). CaCC<sub>inh</sub>-A01 at 80 mg/kg (84 foot lifts) had no significant analgesic effect. Compound **42**, as an ANO1 inhibitor, has a significant analgesic effect on phase 2 but not phase 1 in formalin test, which is consistent with the previous reports<sup>20</sup>.

The chronic constriction injury (CCI) of the sciatic nerve in the rat was used to evaluate the analgesic effects of compounds on the

**Figure 6** The results of *in vivo* analgesic test. (A) Formalin test on rat;  $n = 12$ ; the control group was injected with 50  $\mu$ L saline instead of 5% (v/v) formalin. (B) Chronic constriction injury model (CCI) on rat;  $n = 8$ . Basic represents basic pain threshold before sciatic nerve ligation operation; 0 h, before corresponding compounds treated; 1 h, 1 h after the corresponding compound treated. PTI, the pain threshold rate change (%) of 1 h compared to 0 h. mpk represents mg/kg. All data in (A) and (B) are represented by the mean  $\pm$  SD. Statistical significance was determined by ANOVA, \* $P < 0.05$  and \*\* $P < 0.01$  compared to the vehicle.

nerve injure-derived hyperalgesia. As shown in Fig. 6B, the threshold of paw withdraw measured by Electronic Von Frey before (basic) and after (0 h) CCI model established, and 1 h after compounds administration the threshold of paw withdraw was measured again (1 h). Pregabalin (40 mg/kg) and flupirtine (100 mg/kg) could significantly increase the threshold of paw withdraw with the pain threshold rate change (PTI, %) of 60.4 and 36.2 respectively. Treatment with compound **42** at 40 mg/kg also resulted in a significant analgesic effect (PTI of 45.2), which was more potent than 100 mg/kg flupirtine.

Based on the analgesic effects of ANO1 inhibitor compound **42** in different kinds of pain models, by i.g. administration compound **42** displayed more strength analgesic effects on chronic pain, including formalin-induced allodynia and sciatic nerve ligation-induced mechanical allodynia, especially on inflammation-related chronic pain (phase 2 in formalin test). For acute pain, however, no significant analgesic effect was observed with ANO1 inhibitors treatment in the hot plate test and the writhing test (Supporting Information Figs. S3 and S4).

### 2.9. Binding pose prediction of compound **42**

To get insight into the binding behavior of ANO1 and its inhibitor, a lot of computer-aided drug design work has been conducted. Firstly, the human ANO1 (hANO1) homology modeling of dimer structure (Fig. 7A, Supporting Information) was constructed based

on mANO1 cryo-electron microscopy structure<sup>36–40</sup> using Schrödinger Prime software (sequence alignment results are shown in Supporting Information Fig. S5). Then Schrödinger SiteMap software was used to predict binding sites, and three ligand binding sites were provided (Fig. 7B). Site 1 is located outside the membrane surrounded by the terminals of  $\alpha 5$ ,  $\alpha 6$ , and  $\alpha 9$ . Site 2 is adjacent to the  $\text{Ca}^{2+}$  binding region and consists of  $\alpha 6$ ,  $\alpha 7$ , and  $\alpha 8$ . Site 3 was near the exit of the pore inside the membrane.

Many hydrophilic arginine and glutamine residues enriched in site 3, lead to most of the hydrophobic ANO1 inhibitors were incapable to bind this area, so site 3 was ruled out first. Then reported ANO1 inhibitors (Fig. 1) and compound **42** were docked into site 1 and site 2 to evaluate whether the docking conformation conformed to the corresponding SAR. In site 1, ANO1 inhibitors docking conformation were randomly distributed in the binding pocket around K865, which indicated site 1 volume is too large for these inhibitors to form a stable docking conformation (Fig. 7C). In site 2, all inhibitors showed a very consistent binding conformation (Fig. 7D): the aromatic ring on the carbonyl side of the amide bond was embedded in the hydrophobic loop between  $\alpha 7$  and  $\alpha 8$ , the carboxylic acid kept towards K767. As previously reported<sup>39,40</sup>,  $\alpha 6$  and the calcium-binding region produced large conformational changes during  $\text{Ca}^{2+}$  induced ANO1 activation, thereby compounds binding to this region might be effective to inhibit ANO1. Thereby, site 2 is more likely to be the inhibitors binding site.

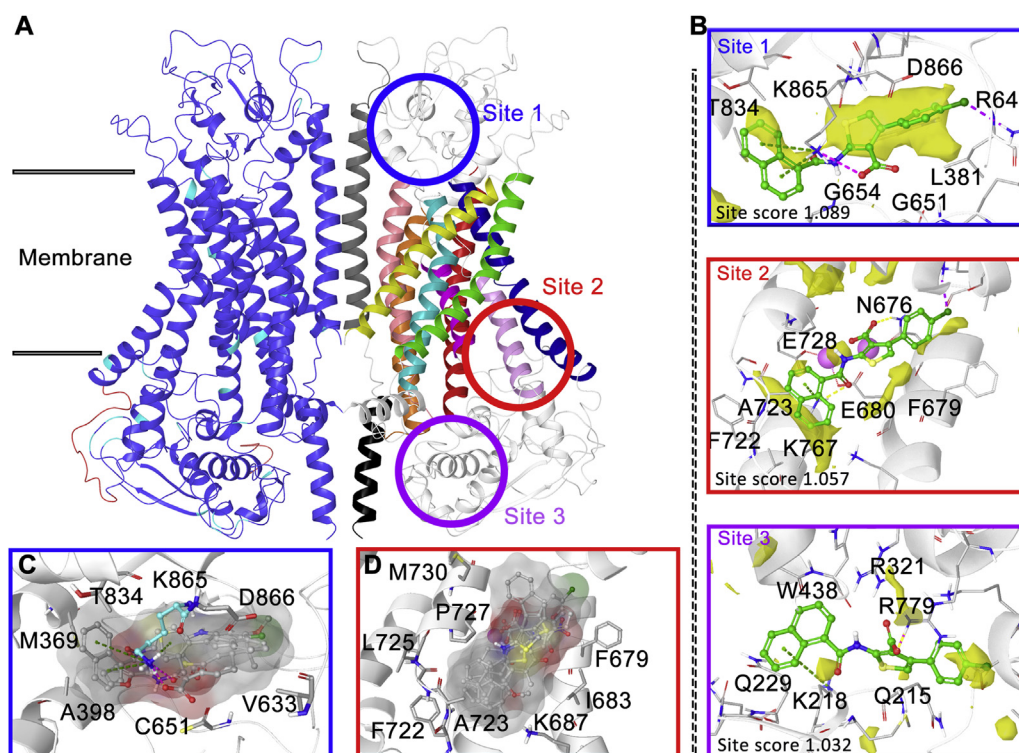


**Figure 7** Homology modeling and binding site prediction of hANO1 protein. (A) Dimer hANO1 homology modeling protein; the colors of left ANO1 monomer represent sequence similarity to the mANO1: dark blue, identical; cyan, similar; red, different; the color of the right monomer represents the hANO1 transmembrane helix: red,  $\alpha 1$ : E326–D361; orange,  $\alpha 2$ : A408–T441; yellow,  $\alpha 3$ : Y516–M544; green,  $\alpha 4$ : T563–E594; cyan,  $\alpha 5$ : K600–K626; dark blue,  $\alpha 6$ : L657–L693; purple,  $\alpha 7$ : T726–T740; pink,  $\alpha 8$ : T752–T770; plum,  $\alpha 9$ : R779–F807; grey,  $\alpha 10$ : N875–W910; black,  $\alpha 11$ : D918–R936. The circles mean the potent ligand binding site predicted by SiteMap software. (B) The results of SiteMap prediction, the yellow surface represents hydrophobic volume. (C) and (D) Docking poses superposition of ANO1 inhibitors to site 1 (C) and site 2 (D).

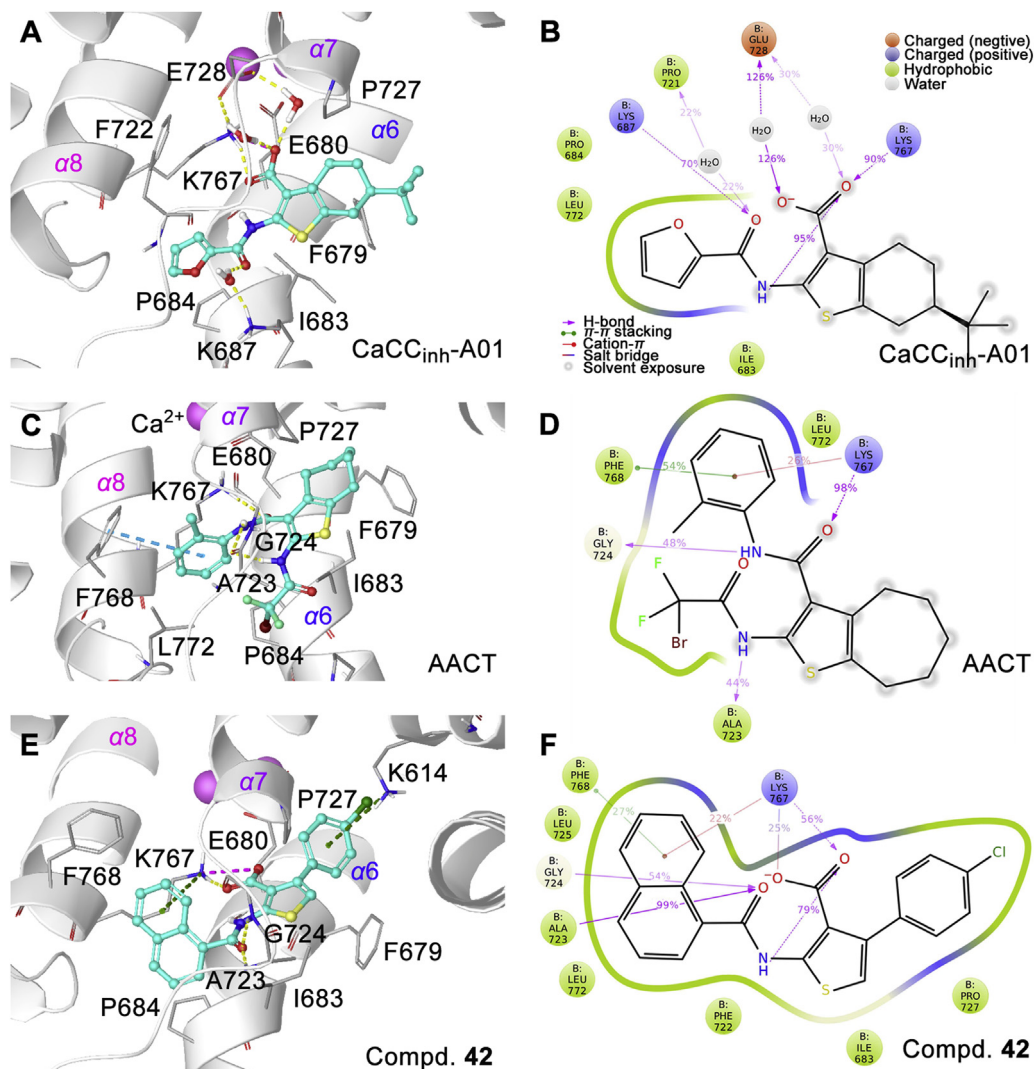


**Figure 8** Interaction pattern of ANO1 inhibitors to hANO1. (A), (C), and (E): The interaction pattern of ANO1-inhibitors; yellow line, hydrogen bond; cyan line,  $\pi$ - $\pi$  stacking; green line, cation- $\pi$  interaction; pink line, electronic interaction. (B), (D), and (F): Interaction diagram during 10–0 ns molecular dynamic simulations. The percentage values on the interaction line represent the time proportion of this interaction over the course of the trajectory: for example, a value of 70% suggests that 70% of the simulation time the specific interaction is maintained. Values over 100% are possible as some protein residue may make multiple contacts of the same subtype with the ligand.

Flexible molecular docking was used to dock the CaCC<sub>inh</sub>-A01, AACT, and compound **42** into the site 2, and 30 ns molecular dynamic simulation was conducted based on docking conformation for more accurate protein–ligand interaction pattern (Fig. 8).

The carboxyl group of compound **42** and CaCC<sub>inh</sub>-A01 formed an electrostatic interaction with K767. Amide in all three compounds formed hydrogen bonds to A723 and G724 main chain. Naphthalene of compound **42** is embedded into the hydrophobic loop between  $\alpha 7$  and  $\alpha 8$  to form the cation- $\pi$  interaction with K767. The 4-chlorophenyl of compound **42** formed the cation- $\pi$  interaction with K614.

To verify the binding site, we mutated the hANO1 residues and constructed a transient ANO1 high expression cell line on HEK293 cells. The differences of inhibition rate of 30  $\mu$ mol/L CaCC<sub>inh</sub>-A01 against wild type ( $69.4 \pm 9.8\%$ , average  $\pm$  SD,  $n = 3$ ) and mutant types were tested in whole-cell patch clamp at +100 mV potential. R321A (in site 3) and K614A (in site 2) mutations did not affect ANO1 inhibitory activity of CaCC<sub>inh</sub>-A01, and K671A (near the Ca<sup>2+</sup> binding pocket) reduced ANO1

inhibition rate of CaCC<sub>inh</sub>-A01 ( $38.0 \pm 13.6\%$ , average  $\pm$  SD,  $n = 3$ ,  $P < 0.05$ ,  $t$ -test). Whereas the mutation of K687A, K767A, and F768A in site 2 changed the electrophysiological features of CaCC current, led to unable to test ANO1 inhibition. Therefore, the uncertainty still exists to reveal the binding site without other experimental evidence such as structural biology.

### 3. Conclusions

Herein, we found a series of thiophenic acid and benzoic acid derivative ANO1 inhibitors by virtual screening. Among which, 4-arylthiophene-3-carboxylic acid scaffold was selected as a hit for further structural optimization, and compound **42** (IC<sub>50</sub> = 790 nmol/L) was obtained. Activity verification showed that compound **42** could strongly inhibit the CaCC current in whole-cell patch clamp, and did not affect ANO2-induced CaCC current and weakly hinder Ca<sup>2+</sup> transmembrane. Furthermore, the preliminary analgesic activity of compound **42** was evaluated in a variety of pain models by i.g. administration. The results showed

that compound **42** had significant analgesic activity on inflammation-related pain. Finally, the binding site of compound **42** to ANO1 was predicted by homology modeling, docking, and molecular dynamics, which suggested that the binding site was close to the Ca<sup>2+</sup> binding region. Our study is the first to show that an oral ANO1 inhibitor has a significant analgesic effect and also provides selective molecular tools for ANO1-related research.

## 4. Experimental

### 4.1. Virtual screening

#### 4.1.1. Ligands and proteins preparation

Ligand preparation was using Schrödinger LigPrep software (2014-2 suites) with the OPLS-2005 force field and default parameters. The SPECS (<http://www.specs.com>) and PKU\_CNCL (<http://www.pkucncl.com>) database were downloads from the website.

#### 4.1.2. Shape and electronic distribution-based virtual screening

Shape and electronic distribution-based virtual screening were based on CaCC<sub>inh</sub>-A01 optimized conformation using ROCs and EON in OPENEYE software. In ROCs, the parameters were set as: “Tanimoto cutoff 0.6, rank by Shape Tanimoto” and in EON, the parameters were set as default.

### 4.2. Chemistry

The screened compounds were purchased from the SPECS database and PKU-CNCL. The purities of all purchased compounds were more than 90%. For the chemical synthesis, reagents and solvents were obtained from J&K Chemical (Beijing, China) without further purification. T16A<sub>inh</sub>-A01 was purchased from TOCRIS (USA). <sup>1</sup>H-NMR and <sup>13</sup>C-NMR spectra were recorded on Bruker (400 MHz) instruments, using DMSO-*d*<sub>6</sub> or CDCl<sub>3</sub> as solvents. High-resolution mass spectra (HRMS) were recorded on the Bruker Apex IV FTMS mass spectrometer using ESI (electrospray ionization). The microwave-assisted reaction was performed on the CEM Discover SP microwave reactor. The purity of the final compound was determined by NMR and HPLC to be >95% (UV detection ( $\lambda = 254$  nm), compound structures in smiles format and more detail can be found in [Supporting Information](#)).

#### 4.2.1. Synthesis of CaCC<sub>inh</sub>-A01

6-(*tert*-Butyl)-2-(furan-2-carboxamido)-4,5,6,7-tetrahydrobenzo [*b*]thiophene-3-carboxylic acid (CaCC<sub>inh</sub>-A01, **1**) was synthesized according to the reported method<sup>24</sup>. Yellow powder, m.p. 205–215 °C. <sup>1</sup>H-NMR (400 MHz, DMSO-*d*<sub>6</sub>)  $\delta$  13.25 (s, 1H), 12.20 (s, 1H), 8.06 (s, 1H), 7.36 (s, 1H), 6.80 (s, 1H), 3.06 (d, *J* = 17.0 Hz, 1H), 2.70 (d, *J* = 14.6 Hz, 1H), 2.45–2.34 (m, 1H), 2.03–1.94 (m, 1H), 1.43 (d, *J* = 5.9 Hz, 1H), 1.32–1.14 (m, 2H), 0.93 (s, 9H). <sup>13</sup>C-NMR (101 MHz, DMSO-*d*<sub>6</sub>)  $\delta$  168.12, 154.62, 147.66, 146.89, 146.56, 132.12, 127.80, 117.44, 113.97, 113.20, 45.29, 33.06, 28.00, 27.84, 26.22, 24.83. HRMS (ESI-TOF<sup>+</sup>) Calcd. for C<sub>18</sub>H<sub>20</sub>NO<sub>4</sub>S [M-H]<sup>-</sup> *m/z*: 346.1113, Found 346.1105.

#### 4.2.2. Synthesis of compounds **33–46**

Taking compound **42** as an example: 4-chloroacetophenone 18.55 g (120 mmol), ethyl cyanoacetate 16.29 g (144 mmol), acetic acid 7.12 g (120 mmol), morpholine 23.00 g (264 mmol),

and ethanol 500 mL were added to a 1 L round bottom flask. Stirred at 68 °C for 3 h under an argon atmosphere, followed by the addition of 4.91 g (144 mmol) sulfur and then stirred for 48 h. The solution was diluted with DCM and washed with brine four times. The organic phase was separated and evaporated 10 mL EA was added to re-dissolve the residue. Acidic EA was added, the precipitates were collected, washed, and then was added to 200 mL 50% ammonia and stirred for 30 min. Followed by extraction with DCM four times, the combined organic phase dried with anhydrous Na<sub>2</sub>SO<sub>4</sub>. After evaporation, 2-aminothiophene-3-carboxylate acid ethyl ester was obtained (yield 21%). 0.195 g (0.73 mmol) 2-aminothiophene-3-carboxylate acid ethyl ester was dissolved in 10 mL DCM, and 0.125 g (0.66 mmol) 1-naphthyl chloride in 10 mL DCM was added at 0 °C. The solution was stirred at room temperature for 8 h, followed by evaporation and recrystallization using DCM/petroleum ether. White powder intermediate 0.227 g (0.54 mmol) was obtained (yield 75%). 0.143 g (0.34 mmol) white powder intermediate and NaOH 0.068 g (1.7 mmol) were dissolved in THF/methanol/water solution and stirred at room temperature for 8 h, acetic acid was used to adjust pH to neutral and water was added to precipitate. 0.094 g (0.23 mmol) **42** was obtained at a yield of 69%.

4.2.2.1. 2-(4-(*tert*-Butyl) benzamido)-4-(4-fluorophenyl) thiophene-3-carboxylic acid (**33**). White powder, m.p. 210–211 °C. Total yield 33%. <sup>1</sup>H-NMR (400 MHz, DMSO-*d*<sub>6</sub>)  $\delta$  12.44 (s, 1H), 7.92 (d, *J* = 8.3 Hz, 2H), 7.69 (d, *J* = 8.3 Hz, 2H), 7.42 (dd, *J* = 8.4, 5.7 Hz, 2H), 7.21 (t, *J* = 8.8 Hz, 2H), 6.97 (s, 1H), 1.36 (s, 9H). <sup>13</sup>C-NMR (101 MHz, DMSO-*d*<sub>6</sub>)  $\delta$  167.62, 163.43, 163.13, 160.71, 156.46, 149.98, 139.05, 134.11, 131.47, 131.39, 129.68, 127.47, 126.56, 116.33, 114.75, 114.54, 112.83, 35.30, 31.24. HRMS (ESI-TOF<sup>+</sup>) Calcd. for C<sub>22</sub>H<sub>19</sub>FNO<sub>3</sub>S [M-H]<sup>-</sup> *m/z*: 396.1070, Found: 396.1070.

4.2.2.2. 2-(4-(*tert*-Butyl) benzamido)-4-(4-chlorophenyl) thiophene-3-carboxylic acid (**34**). White powder, m.p. 245–246 °C. Total yield 30%. <sup>1</sup>H-NMR (400 MHz, DMSO-*d*<sub>6</sub>)  $\delta$  12.43 (s, 1H), 7.92 (d, *J* = 7.7 Hz, 2H), 7.70 (d, *J* = 7.7 Hz, 2H), 7.43 (dd, *J* = 15.8, 7.5 Hz, 4H), 7.01 (s, 1H), 1.37 (s, 9H). <sup>13</sup>C-NMR (101 MHz, DMSO-*d*<sub>6</sub>)  $\delta$  167.48, 163.47, 156.51, 150.03, 138.82, 136.66, 132.23, 131.33, 129.67, 127.87, 127.49, 126.61, 116.63, 112.78, 35.35, 31.28. HRMS (ESI-TOF<sup>+</sup>) Calcd. for C<sub>22</sub>H<sub>19</sub>ClNO<sub>3</sub>S [M-H]<sup>-</sup> *m/z*: 412.0774, Found: 412.0762.

4.2.2.3. 2-(4-(*tert*-Butyl) benzamido)-4-(4-(trifluoromethyl) phenyl) thiophene-3-carboxylic acid (**35**). White powder, m.p. 230–231 °C. Total yield 34%, <sup>1</sup>H-NMR (400 MHz, DMSO-*d*<sub>6</sub>)  $\delta$  12.51 (s, 1H), 7.93 (d, *J* = 8.0 Hz, 2H), 7.72 (dd, *J* = 21.2, 8.0 Hz, 4H), 7.62 (d, *J* = 7.8 Hz, 2H), 7.09 (s, 1H), 1.36 (s, 9H). <sup>13</sup>C-NMR (101 MHz, DMSO-*d*<sub>6</sub>)  $\delta$  167.37, 163.51, 156.53, 150.08, 142.06, 138.67, 130.34, 129.66, 127.52, 126.61, 124.72, 117.29, 112.94, 35.35, 31.27. HRMS (ESI-TOF<sup>+</sup>) *m/z* Calcd. for C<sub>23</sub>H<sub>19</sub>F<sub>3</sub>NO<sub>3</sub>S [M-H]<sup>-</sup> *m/z*: 446.1038, Found: 446.1041.

4.2.2.4. 2-(4-(*tert*-Butyl) benzamido)-4-(4-(*tert*-butyl) phenyl) thiophene-3-carboxylic acid (**36**). Grey powder, m.p. 220–221 °C. Total yield 33%, <sup>1</sup>H-NMR (400 MHz, DMSO-*d*<sub>6</sub>)  $\delta$  12.47 (s, 1H), 7.93 (d, *J* = 7.9 Hz, 2H), 7.69 (d, *J* = 7.9 Hz, 2H), 7.40 (d, *J* = 7.8 Hz, 2H), 7.32 (d, *J* = 7.8 Hz, 2H), 6.92 (s, 1H), 1.36 (s, 9H), 1.34 (s, 9H). <sup>13</sup>C-NMR (101 MHz, DMSO-*d*<sub>6</sub>)

$\delta$  167.74, 163.40, 156.44, 149.87, 149.64, 140.15, 134.88, 129.76, 129.20, 127.48, 126.57, 124.65, 116.00, 112.84, 35.32, 34.69, 31.64, 31.27. HRMS (ESI-TOF<sup>+</sup>)  $m/z$  Calcd. for C<sub>26</sub>H<sub>28</sub>NO<sub>3</sub>S [M-H]<sup>-</sup>  $m/z$ : 434.1790, Found: 434.1793.

4.2.2.5. 4-([1,1'-Biphenyl]-4-yl)-2-(4-(*tert*-butyl) benzamido) thiophene-3-carboxylic acid (**37**). White powder, m.p. 225–226 °C. Total yield 36%, <sup>1</sup>H-NMR (400 MHz, DMSO-*d*<sub>6</sub>)  $\delta$  12.44 (s, 1H), 7.93 (d,  $J$  = 7.5 Hz, 2H), 7.72 (dd,  $J$  = 17.5, 8.1 Hz, 6H), 7.51 (dd,  $J$  = 17.2, 7.9 Hz, 4H), 7.41 (t,  $J$  = 7.2 Hz, 1H), 7.02 (s, 1H), 1.37 (s, 9H). <sup>13</sup>C-NMR (101 MHz, DMSO-*d*<sub>6</sub>)  $\delta$  167.64, 163.49, 156.52, 149.95, 140.33, 139.77, 139.18, 136.93, 130.10, 129.73, 129.44, 127.88, 127.50, 127.03, 126.61, 126.19, 116.37, 112.87, 35.35, 31.28. HRMS (ESI-TOF<sup>+</sup>)  $m/z$  Calcd. for C<sub>28</sub>H<sub>24</sub>NO<sub>3</sub>S [M-H]<sup>-</sup>  $m/z$ : 454.1477, Found: 454.1477.

4.2.2.6. 2-(4-(*tert*-Butyl) benzamido)-4-(2,4-dichlorophenyl) thiophene-3-carboxylic acid (**38**). White powder, m.p. 225–226 °C. Yield 38%, <sup>1</sup>H-NMR (400 MHz, DMSO-*d*<sub>6</sub>)  $\delta$  12.53 (s, 1H), 7.92 (d,  $J$  = 7.1 Hz, 2H), 7.68 (dd,  $J$  = 19.8, 9.0 Hz, 4H), 7.39 (d,  $J$  = 8.1 Hz, 1H), 7.10 (s, 1H), 1.37 (s, 9H). <sup>13</sup>C-NMR (101 MHz, DMSO-*d*<sub>6</sub>)  $\delta$  167.28, 163.52, 156.53, 150.01, 138.49, 137.47, 131.40, 130.48, 130.14, 130.00, 129.97, 129.70, 127.51, 126.62, 117.27, 112.98, 35.36, 31.29. HRMS (ESI-TOF<sup>+</sup>)  $m/z$  Calcd. for C<sub>22</sub>H<sub>18</sub>Cl<sub>2</sub>NO<sub>3</sub>S [M-H]<sup>-</sup>  $m/z$ : 446.0384, Found: 446.0378.

4.2.2.7. 2-(4-(*tert*-Butyl) benzamido)-4-(naphthalen-2-yl) thiophene-3-carboxylic acid (**39**). White powder, m.p. 230–231 °C. Total yield 23%, <sup>1</sup>H-NMR (400 MHz, DMSO-*d*<sub>6</sub>)  $\delta$  12.47 (s, 1H), 8.01–7.87 (m, 6H), 7.71 (d,  $J$  = 7.9 Hz, 2H), 7.56 (s, 3H), 7.09 (s, 1H), 1.37 (s, 9H). <sup>13</sup>C-NMR (101 MHz, DMSO-*d*<sub>6</sub>)  $\delta$  167.65, 163.50, 156.50, 150.01, 140.11, 135.57, 133.06, 132.50, 129.74, 128.60, 128.30, 127.88, 127.51, 127.43, 126.83, 126.62, 126.52, 126.36, 116.63, 113.00, 35.36, 31.29. HRMS (ESI-TOF<sup>+</sup>)  $m/z$  Calcd. for C<sub>26</sub>H<sub>22</sub>NO<sub>3</sub>S [M-H]<sup>-</sup>  $m/z$ : 428.1320, Found: 428.1321.

4.2.2.8. 4-(4-Methoxyphenyl)-2-(thiophene-2-carboxamido) thiophene-3-carboxylic acid (**40**). White powder, m.p. 241–242 °C. Total yield 37%. <sup>1</sup>H-NMR (400 MHz, DMSO-*d*<sub>6</sub>)  $\delta$  12.55 (s, 1H), 8.05 (d,  $J$  = 4.5 Hz, 1H), 7.80 (d,  $J$  = 3.0 Hz, 1H), 7.34 (s, 1H), 7.31 (d,  $J$  = 8.5 Hz, 2H), 6.94 (d,  $J$  = 8.4 Hz, 2H), 6.89 (s, 1H), 3.81 (s, 3H). <sup>13</sup>C-NMR (101 MHz, DMSO-*d*<sub>6</sub>)  $\delta$  167.67, 158.86, 158.48, 139.98, 137.36, 133.81, 130.61, 130.28, 130.01, 129.25, 115.63, 113.34, 55.53. HRMS (ESI-TOF<sup>+</sup>)  $m/z$  Calcd. for C<sub>17</sub>H<sub>12</sub>NO<sub>4</sub>S<sub>2</sub> [M-H]<sup>-</sup>  $m/z$ : 358.0208, Found: 358.0207.

4.2.2.9. 4-(4-(*tert*-Butyl) phenyl)-2-(4-methoxybenzamido) thiophene-3-carboxylic acid (**41**). White powder, m.p. 215–216 °C. Total yield 30%, <sup>1</sup>H-NMR (400 MHz, DMSO-*d*<sub>6</sub>)  $\delta$  12.44 (s, 1H), 7.95 (d,  $J$  = 8.2 Hz, 2H), 7.40 (d,  $J$  = 7.6 Hz, 2H), 7.32 (d,  $J$  = 7.9 Hz, 2H), 7.21 (d,  $J$  = 8.2 Hz, 2H), 6.91 (s, 1H), 3.90 (s, 3H), 1.34 (s, 9H). <sup>13</sup>C-NMR (101 MHz, DMSO-*d*<sub>6</sub>)  $\delta$  167.77,

163.34, 163.02, 150.05, 149.62, 140.10, 134.91, 129.59, 129.19, 124.65, 124.56, 115.85, 115.04, 112.64, 56.08, 34.70, 31.64. HRMS (ESI-TOF<sup>+</sup>)  $m/z$  Calcd. for C<sub>23</sub>H<sub>22</sub>NO<sub>4</sub>S [M-H]<sup>-</sup>  $m/z$ : 408.1270, Found: 408.1268.

4.2.2.10. 2-(1-Naphthamido)-4-(4-chlorophenyl) thiophene-3-carboxylic acid (**42**). Colorless crystal, m.p. 241–242 °C. Total yield 17%. <sup>1</sup>H-NMR (400 MHz, DMSO-*d*<sub>6</sub>)  $\delta$  12.11 (s, 1H), 8.47 (d,  $J$  = 7.7 Hz, 1H), 8.24 (d,  $J$  = 8.0 Hz, 1H), 8.11 (d,  $J$  = 7.3 Hz, 1H), 8.02 (d,  $J$  = 6.8 Hz, 1H), 7.71 (dd,  $J$  = 14.0, 6.8 Hz, 3H), 7.43 (q,  $J$  = 7.6 Hz, 4H), 7.08 (s, 1H). <sup>13</sup>C-NMR (101 MHz, DMSO-*d*<sub>6</sub>)  $\delta$  167.07, 165.67, 149.32, 138.85, 136.61, 133.89, 132.59, 132.27, 131.83, 131.30, 130.12, 129.10, 128.18, 127.92, 127.28, 126.75, 125.66, 125.33, 116.82, 113.44. HRMS (ESI-TOF<sup>+</sup>)  $m/z$  Calcd. for C<sub>22</sub>H<sub>13</sub>ClNO<sub>3</sub>S [M-H]<sup>-</sup>  $m/z$ : 406.0305, Found: 406.0305.

4.2.2.11. 2-(2-Naphthamido)-4-(4-chlorophenyl) thiophene-3-carboxylic acid (**43**). White powder, m.p. 240–241 °C. Total yield 14%, <sup>1</sup>H-NMR (400 MHz, DMSO-*d*<sub>6</sub>)  $\delta$  12.94 (s, 1H), 8.61 (s, 1H), 8.16 (d,  $J$  = 6.5 Hz, 2H), 8.05 (dd,  $J$  = 18.1, 8.3 Hz, 2H), 7.70 (dt,  $J$  = 19.4, 7.0 Hz, 2H), 7.44 (s, 4H), 7.02 (s, 1H). <sup>13</sup>C-NMR (101 MHz, DMSO-*d*<sub>6</sub>)  $\delta$  167.49, 163.59, 149.62, 139.02, 136.75, 135.19, 132.67, 132.16, 131.36, 129.91, 129.67, 129.46, 128.98, 128.69, 128.24, 127.84, 127.75, 123.55, 116.57, 113.81. HRMS (ESI-TOF<sup>+</sup>)  $m/z$  Calcd. for C<sub>22</sub>H<sub>13</sub>ClNO<sub>3</sub>S [M-H]<sup>-</sup>  $m/z$ : 406.0305, Found: 406.0304.

4.2.2.12. 4-(4-Chlorophenyl)-2-(2,4-dichlorobenzamido) thiophene-3-carboxylic acid (**44**). White powder, m.p. 239–240 °C. Total yield 24%, <sup>1</sup>H-NMR (400 MHz, DMSO-*d*<sub>6</sub>)  $\delta$  12.07 (s, 1H), 7.88 (s, 2H), 7.67 (d,  $J$  = 8.3 Hz, 1H), 7.42 (dd,  $J$  = 20.3, 7.6 Hz, 4H), 7.08 (s, 1H). <sup>13</sup>C-NMR (101 MHz, DMSO-*d*<sub>6</sub>)  $\delta$  166.70, 162.51, 148.18, 138.87, 137.15, 136.46, 132.63, 132.29, 132.07, 131.95, 131.24, 130.51, 128.55, 127.93, 117.18, 114.21. HRMS (ESI-TOF<sup>+</sup>)  $m/z$  Calcd. for C<sub>18</sub>H<sub>9</sub>Cl<sub>3</sub>NO<sub>3</sub>S [M-H]<sup>-</sup>  $m/z$ : 423.9369, Found: 423.9368.

4.2.2.13. 4-(4-Chlorophenyl)-2-(thiophene-2-carboxamido) thiophene-3-carboxylic acid (**45**). White powder, m.p. 225–226 °C. Total yield 22%. <sup>1</sup>H-NMR (400 MHz, DMSO-*d*<sub>6</sub>)  $\delta$  12.40 (s, 1H), 8.05 (d,  $J$  = 4.8 Hz, 1H), 7.81 (s, 1H), 7.42 (q,  $J$  = 8.1 Hz, 4H), 7.35 (t,  $J$  = 3.7 Hz, 1H), 7.00 (s, 1H). <sup>13</sup>C-NMR (101 MHz, DMSO-*d*<sub>6</sub>)  $\delta$  167.39, 158.49, 149.49, 138.83, 137.07, 136.54, 134.02, 132.25, 131.32, 130.43, 129.29, 127.87, 116.75, 113.01. HRMS (ESI-TOF<sup>+</sup>)  $m/z$  Calcd. for C<sub>16</sub>H<sub>9</sub>ClNO<sub>3</sub>S<sub>2</sub> [M-H]<sup>-</sup>  $m/z$ : 361.9712, Found: 361.9715.

4.2.2.14. 4-(4-Chlorophenyl)-2-(4-methyl-1-naphthamido) thiophene-3-carboxylic acid (**46**). White powder, m.p. 250–251 °C. Total yield 24%, <sup>1</sup>H-NMR (400 MHz, DMSO-*d*<sub>6</sub>)  $\delta$  12.08 (s, 1H), 8.51 (s, 1H), 8.20 (s, 1H), 7.91 (d,  $J$  = 6.8 Hz, 1H), 7.72 (s, 2H), 7.58 (d,  $J$  = 6.4 Hz, 1H), 7.43 (d,  $J$  = 8.8 Hz, 4H), 7.07 (s, 1H), 2.79 (s, 3H). <sup>13</sup>C-NMR (101 MHz, DMSO-*d*<sub>6</sub>)  $\delta$  167.10, 165.79, 149.49, 139.54, 138.82, 136.64, 132.87, 132.25, 131.30, 130.25, 130.15, 127.91, 127.82, 127.23, 126.50, 126.25, 125.88, 125.24,

116.73, 113.22, 19.92. HRMS (ESI-TOF<sup>+</sup>) *m/z* Calcd. for C<sub>23</sub>H<sub>15</sub>ClNO<sub>3</sub>S [M-H]<sup>-</sup> *m/z*: 420.0461, Found: 420.0454.

#### 4.2.3. Synthesis of compounds 47–53

Taking compound **48** as an example. Indanone 1.409 g (8.0 mmol), ethyl cyanoacetate 1.352 g (9.6 mmol), acetic acid 0.480 g (9.6 mmol), ammonium acetate 0.736 g (9.6 mmol), and toluene 100 mL were added into a round bottom flask and refluxed for 8 h. After evaporation, morpholine 0.832 g (76.8 mmol), sulfur 0.384 g (9.6 mmol), and ethanol 100 mL were added and stirred for 48 h at 80 °C under an argon atmosphere. The reaction solution was diluted with 150 mL DCM, washed with brine four times, and dried with anhydrous Na<sub>2</sub>SO<sub>4</sub>. After evaporation and column chromatography purification, brown solid immediate was obtained (yield, 35%). The following procedures were the same as compound **42**. Finally, the brown powder compound **48** was obtained.

4.2.3.1. 2-(4-(*tert*-Butyl) benzamido)-8*H*-indeno [2,1-*b*] thiophene-3-carboxylic acid (**47**). Yellowish powder, m.p. 260–261 °C. Yield 25%. <sup>1</sup>H-NMR (400 MHz, DMSO-*d*<sub>6</sub>) δ 12.48 (s, 1H), 8.25 (d, *J* = 7.7 Hz, 1H), 7.84 (d, *J* = 7.9 Hz, 2H), 7.60 (d, *J* = 8.0 Hz, 2H), 7.46 (d, *J* = 7.3 Hz, 1H), 7.28 (t, *J* = 7.5 Hz, 1H), 7.17 (d, *J* = 7.4 Hz, 1H), 3.80 (s, 2H), 1.29 (s, 9H). <sup>13</sup>C-NMR (101 MHz, DMSO-*d*<sub>6</sub>) δ 167.80, 163.17, 156.38, 152.32, 147.03, 140.72, 138.97, 136.13, 129.68, 127.45, 126.90, 126.53, 125.13, 124.84, 122.63, 107.92, 35.32, 34.50, 31.26. HRMS (ESI-TOF<sup>+</sup>) *m/z* Calcd. for C<sub>23</sub>H<sub>20</sub>NO<sub>3</sub>S [M-H]<sup>-</sup> *m/z*: 390.1164, Found: 390.1165.

4.2.3.2. 2-(4-(*tert*-Butyl) benzamido)-6-methoxy-8*H*-indeno [2,1-*b*] thiophene-3-carboxylic acid (**48**). Brown powder, m.p. 213–214 °C. Total yield 19%. <sup>1</sup>H-NMR (400 MHz, DMSO-*d*<sub>6</sub>) δ 12.48 (s, 1H), 8.15 (d, *J* = 8.6 Hz, 1H), 7.89 (d, *J* = 8.0 Hz, 2H), 7.66 (d, *J* = 8.0 Hz, 2H), 7.14 (s, 1H), 6.90 (d, *J* = 8.5 Hz, 1H), 3.82 (s, 2H), 3.78 (s, 3H), 1.34 (s, 9H). <sup>13</sup>C-NMR (101 MHz, DMSO-*d*<sub>6</sub>) δ 167.83, 163.11, 157.78, 156.39, 152.01, 148.98, 140.63, 133.79, 131.98, 129.74, 127.44, 126.57, 123.09, 112.43, 111.21, 107.74, 55.67, 35.34, 34.65, 31.29. HRMS (ESI-TOF<sup>+</sup>) *m/z* Calcd. for C<sub>24</sub>H<sub>22</sub>NO<sub>4</sub>S [M-H]<sup>-</sup> *m/z*: 420.1270, Found: 420.1263.

4.2.3.3. 2-(Thiophene-2-carboxamido)-8*H*-indeno [2,1-*b*] thiophene-3-carboxylic acid (**49**). Brown powder, m.p. 245–246 °C. Total yield 21%. <sup>1</sup>H-NMR (400 MHz, DMSO-*d*<sub>6</sub>) δ 8.33 (d, *J* = 7.7 Hz, 1H), 8.04 (d, *J* = 4.8 Hz, 1H), 7.81 (d, *J* = 2.7 Hz, 1H), 7.53 (d, *J* = 7.3 Hz, 1H), 7.35 (t, *J* = 7.2 Hz, 2H), 7.23 (t, *J* = 7.4 Hz, 1H), 3.88 (s, 2H). <sup>13</sup>C-NMR (101 MHz, DMSO-*d*<sub>6</sub>) δ 167.75, 158.24, 151.76, 147.00, 140.82, 138.96, 137.22, 136.19, 133.88, 130.27, 129.25, 126.90, 125.16, 124.84, 122.67, 108.30, 34.56. HRMS (ESI-TOF<sup>+</sup>) *m/z* Calcd. for C<sub>17</sub>H<sub>10</sub>NO<sub>3</sub>S<sub>2</sub> [M-H]<sup>-</sup> *m/z*: 340.0102 Found: 340.0104.

4.2.3.4. 2-(2-Naphthamido)-8*H*-indeno [2,1-*b*] thiophene-3-carboxylic acid (**50**). Greenish powder, m.p. 260–261 °C. Total yield 14%. <sup>1</sup>H-NMR (400 MHz, DMSO-*d*<sub>6</sub>) δ 12.70 (s, 1H), 8.58 (s, 1H), 8.32 (d, *J* = 7.5 Hz, 1H), 8.14 (s, 2H), 8.02 (dd, *J* = 28.5, 7.8 Hz, 2H), 7.69 (t, *J* = 7.1 Hz, 2H), 7.52 (d,

*J* = 7.0 Hz, 1H), 7.35 (t, *J* = 7.2 Hz, 1H), 7.23 (t, *J* = 7.0 Hz, 1H), 3.87 (s, 2H). <sup>13</sup>C-NMR (101 MHz, DMSO-*d*<sub>6</sub>) δ 167.81, 163.29, 152.24, 147.03, 140.76, 138.94, 136.31, 135.16, 132.64, 129.70, 129.65, 129.43, 128.97, 128.72, 128.23, 127.74, 126.91, 125.16, 124.85, 123.38, 122.63, 108.12, 34.52. HRMS (ESI-TOF<sup>+</sup>) *m/z* Calcd. for C<sub>23</sub>H<sub>14</sub>NO<sub>3</sub>S [M-H]<sup>-</sup> *m/z*: 384.0694, Found: 384.0694.

4.2.3.5. 2-(1-Naphthamido)-8*H*-indeno [2,1-*b*] thiophene-3-carboxylic acid (**51**). Yellowish powder, m.p. 265–266 °C. Total yield 17%. <sup>1</sup>H-NMR (400 MHz, DMSO-*d*<sub>6</sub>) δ 12.28 (s, 1H), 8.52 (d, *J* = 7.9 Hz, 1H), 8.34 (d, *J* = 7.6 Hz, 1H), 8.20 (d, *J* = 8.1 Hz, 1H), 8.05 (dd, *J* = 25.0, 7.1 Hz, 2H), 7.68 (t, *J* = 7.5 Hz, 3H), 7.53 (d, *J* = 7.1 Hz, 1H), 7.35 (t, *J* = 7.3 Hz, 1H), 7.24 (t, *J* = 7.1 Hz, 1H), 3.88 (s, 2H). <sup>13</sup>C-NMR (101 MHz, DMSO-*d*<sub>6</sub>) δ 167.47, 165.31, 151.68, 147.06, 140.83, 138.99, 136.27, 133.91, 132.57, 131.72, 130.17, 129.06, 128.12, 127.22, 126.91, 126.74, 125.60, 125.41, 125.16, 124.85, 122.69, 108.55, 34.51. HRMS (ESI-TOF<sup>+</sup>) *m/z* Calcd. for C<sub>23</sub>H<sub>14</sub>NO<sub>3</sub>S [M-H]<sup>-</sup> *m/z*: 384.0694, Found: 384.0685.

4.2.3.6. 2-(4-(*tert*-Butyl) benzamido)-8,8-dimethyl-8*H*-indeno [2,1-*b*] thiophene-3-carboxylic acid (**52**). Brown powder, m.p. 264–265 °C. Total yield 24%. <sup>1</sup>H-NMR (400 MHz, DMSO-*d*<sub>6</sub>) δ 12.56 (s, 1H), 8.26 (d, *J* = 7.5 Hz, 1H), 7.93 (d, *J* = 7.7 Hz, 2H), 7.69 (d, *J* = 6.7 Hz, 2H), 7.54 (d, *J* = 7.1 Hz, 1H), 7.30 (dt, *J* = 26.0, 7.0 Hz, 2H), 1.52 (s, 6H), 1.36 (s, 9H). <sup>13</sup>C-NMR (101 MHz, DMSO-*d*<sub>6</sub>) δ 167.80, 163.22, 157.01, 156.45, 151.83, 147.54, 136.85, 136.70, 129.76, 127.48, 127.28, 126.60, 125.79, 122.81, 122.33, 108.15, 35.34, 31.28, 27.46. HRMS (ESI-TOF<sup>+</sup>) *m/z* Calcd. for C<sub>25</sub>H<sub>24</sub>NO<sub>3</sub>S [M-H]<sup>-</sup> *m/z*: 418.1477, Found: 418.1468.

4.2.3.7. 2-(4-(*tert*-Butyl) benzamido)-4,5-dihydronaphtho [2,1-*b*] thiophene-1-carboxylic acid (**53**). White powder, m.p. 255–256 °C. Total yield 24%. <sup>1</sup>H-NMR (400 MHz, CDCl<sub>3</sub>) δ 11.98 (s, 1H), 8.06 (s, 2H), 7.94 (d, *J* = 8.1 Hz, 2H), 7.67 (d, *J* = 8.1 Hz, 1H), 7.56 (d, *J* = 8.1 Hz, 2H), 7.20 (d, *J* = 7.0 Hz, 1H), 2.95 (t, *J* = 7.0 Hz, 2H), 2.76 (t, *J* = 6.9 Hz, 2H), 1.38 (s, 9H). <sup>13</sup>C-NMR (101 MHz, CDCl<sub>3</sub>) δ 171.98, 163.89, 157.61, 156.56, 135.99, 131.85, 131.33, 130.13, 129.35, 127.65, 127.36, 127.01, 126.51, 126.16, 126.10, 125.51, 77.35, 77.24, 77.04, 76.72, 35.21, 35.17, 31.13, 31.11, 30.28, 23.61, 1.04. HRMS (ESI-TOF<sup>+</sup>) *m/z* Calcd. for C<sub>24</sub>H<sub>22</sub>NO<sub>3</sub>S [M-H]<sup>-</sup> *m/z*: 404.1320, Found: 404.1313.

### 4.3. Biological experiments

#### 4.3.1. Cell culture and reagents

Fischer rat thyroid (FRT) cells stably co-expressing ANO1 isoform (abc) and the halide-sensitive yellow fluorescent protein (YFP)-H148Q/I152L/F46L were kindly provided by Dr. Luis J.V. Galletta (Laboratorio di Genetica Molecolare, Istituto Giannina Gaslini, Genova, Italy) and were maintained in F12 medium containing 10% (v/v) fetal bovine serum (FBS), 1% (v/v) penicillin/streptomycin (P/S). HEK-293T and CHO cells were cultured in DMEM containing 10% (v/v) FBS, 1% (v/v) P/S. The cells were cultured at 37 °C with 5% CO<sub>2</sub> in a humidified incubator. For plate

reader assays, cells were plated in black 96-well microplates (3603, Corning, USA) and assayed 24 h after plating.

FBS (10270-106, Gibco, USA), F12 medium (11765-054, Gibco), 1% (v/v) P/S (CC004, Macgene, China), DMEM (CM10013, Macgene, China). ANO1 inhibitors, CaCC<sub>inh</sub>-A01 and T16A<sub>inh</sub>-A01 (Sigma, USA), Ani9 (Tocris, USA) were dissolved in DMSO to a stock concentration of 10 mmol/L.

#### 4.3.2. Electrophysiology

ANO1 currents were recorded from whole cell patches at room temperature from ANO1-YFP stably co-expressing FRT cell line. The pipet (extracellular) solution contained (in mmol/L) 140 NaCl, 4 KCl, 2 CaCl<sub>2</sub>, 1 MgCl<sub>2</sub>, 10 glucose, and 10 Hepes (pH 7.4). The bath (intracellular) solution A contained (in mmol/L) 146 CsCl, 2 MgCl<sub>2</sub>, 10 sucrose and 8 Hepes (adjusting pH to 7.3 with NMDG). The bath (intracellular) solution B contained (in mmol/L) 146 CsCl, 2 MgCl<sub>2</sub>, 5 CaCl<sub>2</sub>, 5 EGTA, 10 sucrose, and 8 Hepes (adjusting pH to 7.3 with NMDG). Mix the bath solution A and B ( $V_A:V_B = 892:108$ ) to obtain the desired solution with 1 μmol/L free Ca<sup>2+</sup> concentration. The electrical resistance of micropipettes was 3–5 MΩ. Recordings were made using the HEKA EPC10 amplifier with PatchMaster software. The method of ANO1 whole-cell patch clamp is similar to the reference<sup>10,41</sup>. ANO1 was activated by 1 μmol/L free Ca<sup>2+</sup> in the bath solution. The protocol for stimulation consisted of 850 ms voltage steps including +100 to −100 mV (400 ms) starting from a holding potential of 0 mV (50 ms).

ANO2 currents were recorded from whole cell patches at room temperature from ANO2 transiently expressing HEK293 cell line. The protocol, pipet solution, and bath solution are the same as the reference<sup>35</sup>. HEK293 cells were depolarized from the holding potential of −40 mV to test potentials (+100 to −80 mV) by +20 mV increment for 500 ms and subsequently repolarized to −80 mV for 250 ms every 15 s.

#### 4.3.3. YFP fluorescence quenching assay

The method of YFP fluorescence quenching assay is similar to the reference<sup>10,41</sup>. The ANO1-overexpressed FRT cell line was plated in 96-well plates and washed with PBS three times, and incubated with 60 μL test compound/PBS solution for 1 h (PBS with 0.1% (v/v) DMSO as a negative control). The fluorescence was measured in Microplate Reader (Flexstation 3, Molecular Devices) at a frequency of once per 1.7 s for 120 s ( $\lambda_{ex}/\lambda_{em}$ : 514 nm/535 nm). During the measurement, baseline fluorescence data  $F_0$  was collected for 17 s before the addition of a PBS-iodide solution (PBS with 100 mmol/L NaI) containing 200 μmol/L ATP. Fluorescence–time curve was fitted by Eq. (2):

$$F_t/F_0 = \hat{e}(ax^2 + bx + c) \quad (2)$$

The slope was calculated from 5 to 6 points where the fluorescence starts to decrease after adding the PBS-iodide solution. The inhibition rate was calculated by Eq. (1) which is described in Section 2.2. IC<sub>50</sub> was calculated from the inhibition–concentration curve fitted by the Hill equation. Data regulation and calculation were performed with Origin 8 software. Inhibition rate–concentration curves of compounds are in Supporting Information Fig. S2.

#### 4.3.4. Intracellular Ca<sup>2+</sup> fluorescence

HEK-293T cells were plated in 96-well plates and cultured for 24 h before changing the medium of each well into 100 μL

DMEM with 10% (w/v) F127 and 10 μmol/L cal520<sup>TM</sup>. After 2 h incubation, the cells were washed with PBS and incubated for 0.5 h with 100 μL compound/PBS solution at 30 μmol/L compound concentration. Cells were imaged before and 5 s after the addition of 200 μmol/L ATP containing PBS under Nikon eclipse Ti-S inverted fluorescence microscope with the FITC filter, and the data were analyzed with ImageJ software.

#### 4.3.5. Stability under different pH conditions

The target compounds were diluted to 100 μmol/L with pH 1.0, 4.0, 6.8, 7.4, and 9.0 buffers, and the 0 h peak area of the target compounds were obtained by HPLC–UV analysis. Then each pH compound solution was placed in 37 °C water bath. The peak areas of the target compounds were obtained at 2 and 5 h. The change rate in the peak area was obtained by comparing the peak area of the target compound at different times with the peak area of 0 h. pH phosphate buffers were purchased from Shanghai Rongbai Biological Technology Ltd. (Shanghai, China).

#### 4.3.6. MDCK cells permeability

A resistance-stable MDCK monolayer cell model was established in the transwell. A 100 μL compound solution was added to the upper chamber of the transwell, and 0.6 mL HBSS was added to the lower chamber, followed by incubation for 120 min at 37 °C and 5% CO<sub>2</sub>. Then the lower chamber liquid was detected by LC–MS (G6120B, Agilent Technologies, USA), and the compound concentration was calculated. The apparent permeability coefficient was calculated according to Eq. (3):

$$P_{app}(\text{cm/s}) = \Delta Q \times (\Delta t \times A \times C_0) \quad (3)$$

$\Delta Q$  (μg) is the compound transport amount in  $\Delta t$  (s),  $A$  (cm<sup>2</sup>) is the membrane area, and  $C_0$  (μg/mL) is the initial drug concentration in the upper chamber of MDCK cells.

#### 4.3.7. Cytotoxicity

The effect of ANO1 inhibitors on cell viability was determined by the SRB (sulforhodamine B) assay. Briefly, cells were cultured on sterile slides in 96-well plates overnight at 37 °C with 5% CO<sub>2</sub>. Then cells were treated with various dosages of compounds or medium containing 0.5% (v/v) DMSO (control) for 72 h, 200 μL 10% (v/v) trichloroacetic acid (TCA) was added to each well, followed by incubation for 1 h at 4 °C in a refrigerator. After the microplate was washed five times with sterile water, evaporation in air, 100 mL of 0.4% SRB dissolved in 1% (v/v) acetic acid was added to each well. Following an additional incubation at room temperature in the dark for 15 min. After the microplate was washed five times with 1% (v/v) acetic acid, evaporation in air, add 100 mL 10 mmol/L Tris-base to each well to dissolve SRB for 30 min. Absorbance was measured at 540 nm using a microplate reader.

#### 4.3.8. Acute toxicity

The acute toxicity was evaluated by i.g. administration of 1000 mg/kg doses of individual compound **42** into C57BL/6 mice. The C57BL/6 mice (weight, 18–22 g; age, 6–8 weeks; 7 mice per group; male) were purchased from Vital River Laboratories (Beijing, China). 5% (v/v) DMSO+10% (v/v) Glutol+85% (v/v) saline (adjust pH to 8.0 by 1 mol/L NaOH) were used for i.g. administration. Survival was monitored daily for 3 days. All animal experiments were performed in full compliance with the

protocols approved by the Animal Ethics Committee of the Institute of Medicinal Biotechnology (Beijing, China).

#### 4.4. *In vivo pharmacodynamics*

##### 4.4.1. *Animal and treatment*

Animal welfare is in accordance with the Guide for the Care and Use of Laboratory Animals (8th ed., 2011). All animals were purchased from Shanghai Sppr bk laboratory animals Ltd. (Shanghai, China), and fed in SPF animal laboratories. All of *in vivo* experiments were conducted by i.g. administration.

Pregabalin, flupirtine, and morphine hydrochloride injection were obtained from Jiangsu Ehwa Pharmaceutical Group Co., Ltd. PEG400 was purchased from Weier Huagong (Nanjing, China). Administration volume was 1 mL/100 g mouse or rat weight. Most of the compounds in pharmacodynamics tests were conducted by i.g. administration, except for morphine by intraperitoneal (i.p.) administration. Formulation (take 80 mg/kg as example): 80 mg compound **42** sodium salt was dissolved in 2.0 mL DMSO (Bidepharm, Shanghai, China), then diluted in 8.0 mL 30% (v/v) PEG400/saline (Bidepharm), ultrasonic mixing. 8 mg/mL compound **42** sodium salt solution was obtained. Fluoxetine, pregabalin and CaCC<sub>inh</sub>-A01 were also prepared using that same method.

##### 4.4.2. *Formalin test*

The formalin experiment with reference to the experimental method was reported by Okuda et al.<sup>42</sup> 12 SD rats (male, 220–300 g) in each group. The control group and the vehicle group were administered with normal saline. After 30 min, 5% (v/v) formalin 50  $\mu$ L was injected into the rat's left-hand foot in the vehicle group and compound group, and 50  $\mu$ L normal saline was injected in the control group. Then, the number of pain responses (foot lifting) was immediately observed and recorded. 0–10 min after the formalin injection was defined as Phase 1, and 10–60 min was defined as Phase 2. SPSS statistical software was used for data analysis.

##### 4.4.3. *Chronic constriction injury model*

8 SD rats (male, 6–8 weeks, 180–200 g) in each group. The rat's right hind sciatic nerve was ligation to make CCI model according to the method reported by Chaplan et al.<sup>43–45</sup> Paw withdrawal threshold (PWT) was measured 14 days after surgery to evaluate the success of the CCI model (at least 25% lower than before the operation). The PWT was measured 1 h after compound administration. The electronic ciliary instrument used Electronic Von Frey 2390 (IITC Life Science Inc., Woodland Hills, CA, USA). The rate of pain threshold increase (PTI) was calculated as comparable data represent the analgesic effect of different compounds according to Eq. (4):

$$PTI (\%) = (PWT_{0h} - PWT_{1h}) / PWT_{0h} \times 100 \quad (4)$$

PWT<sub>0h</sub> means pain withdraw threshold before compound administration; PWT<sub>1h</sub> means pain withdraws threshold 1 h after compound administration.

##### 4.4.4. *Hot plate test*

The hot plate test method is based on that previously reported by Masocha<sup>46</sup>. 10 ICR mice (female, 6–8 weeks, 18–24 g) in each group. The hot plate temperature was 60 °C; The Latency record as the time between mice contacted with a hot plate to pain response appeared (foot lifting and jumping) before (0 h) and 3 h

after compound administration. The max positive effect (MPE, %) which represents the compound analgesic capability was calculated as Eq. (5):

$$MPE (\%) = (Lat_{0h} - Lat_{3h}) / (60 - Lat_{0h}) MPE\%T \quad (5)$$

Lat means latency, statistical significance was determined by a paired *t*-test between 0 and 3 h in each mice.

##### 4.4.5. *Writhing test*

10 ICR mice (female and male mice (1:1), 6–8 weeks, 18–24 g) each group. The compounds were administered by i.g. administration, and 1 h later, 0.6% (v/v) acetic acid solution was injected by i.p. administration. The number of body writhing was observed and recorded in 15 min. The inhibition rate of compounds was calculated as Eq. (6):

$$\text{Inhibition rate } (\%) = (N_{\text{vehicle}} - N_{\text{comp}}) / N_{\text{vehicle}} \times 100 \quad (6)$$

$N_{\text{vehicle}}$  means the number of writhing in the vehicle group;  $N_{\text{comp}}$  means the number of writhing in compound treated group; one-way ANOVA was used for intergroup comparison and a paired *t*-test was used for intra-group comparison.

#### 4.5. *Binding site analysis*

##### 4.5.1. *Homology modeling*

The protein sequences of human ANO family (hANO1–hANO10) were downloaded from Uniprot website (<https://www.uniprot.org/>). mANO1 protein (PDB code: 5OYB) was downloaded from the PDB database (<http://www.rcsb.org/>) and used as the template. ANO family and mANO1 sequences were aligned automatically in the Schrödinger Prime software. Protein was minimized based on molecular force field (OPLS\_3, 5000 steps), then 15 ns molecular dynamics simulation was made by Schrödinger Desmond software (constrain the main chain atomic coordinates, TIP3P water model, POPC membrane model, charge neutrality, adding 0.15 mol/L NaCl, NPT model, temperature 300 K, and pressure 101.325 bar). The PDB-formatted coordinate files of the hANO1 homology modeling structure were recorded in the Supporting Information Fig. S5.

##### 4.5.2. *Binding site prediction*

The binding site was predicted by the Schrödinger SiteMap component (default parameters). Schrödinger Glide XP (OPLS\_3 force field, no constrains) was used for molecular docking. Induced Fit Docking (standard precision, Glide XP for refinement) in Schrödinger software was used to dock ANO1 inhibitors to hANO1. Based on the binding pose, 50 ns molecular dynamics simulation was conducted by the Schrödinger Desmond software (TIP3P water model, POPC membrane model, charge neutrality, adding 0.15 mol/L NaCl, NPT model, temperature 300 K, and pressure 101.325 bar).

#### Acknowledgments

This research was supported by the National Key Research and Development Project (Grant No. 2019YFC1708900), the National Natural Science Foundation of China (Grant No. 21772005), National Major Scientific and Technological Special Project for Significant New Drugs Development (2019ZX09204-001, China) and Beijing Municipal Natural Science Foundation (7202088, 7172118, China). We are very appreciative of Dr. Wei Huang (Chinese Academy of Medical Sciences) and Dr. Peilin Yu



(Zhejiang University, Hangzhou, China) for their help in this work.

### Author contributions

Yuxi Wang contributed on conceptualization, investigation, formal analysis, software, and writing—original draft. Jian Gao contributed on conceptualization, methodology, investigation, formal analysis. Song Zhao contributed on methodology, investigation, formal analysis. Yan Song contributed on methodology. Han Huang contributed on investigation. Guiwang Zhu contributed on investigation. Peili Jiao contributed on investigation. Xiangqing Xu contributed on resources. Guisen Zhang contributed on resources. Kewei Wang contributed on resources, supervision. Liangren Zhang: contributed on supervision, writing—review & editing. Zhenming Liu contributed on supervision, writing—review & editing.

### Conflicts of interest

The authors have no conflicts of interest to declare.

### Appendix A. Supporting information

Supporting information to this article can be found online at <https://doi.org/10.1016/j.apsb.2020.11.004>.

### References

- Manoury B, Tamuleviciute A, Tammaro P. TMEM16A/Anoctamin 1 protein mediates calcium-activated chloride currents in pulmonary arterial smooth muscle cells. *J Physiol* 2010;**588**:2305–14.
- Ousingsawat J, Martins JR, Schreiber R, Rock JR, Harfe BD, Kunzelmann K. Loss of TMEM16A causes a defect in epithelial  $\text{Ca}^{2+}$ -dependent chloride transport. *J Biol Chem* 2009;**284**:28698–703.
- Rock JR, O'Neal WK, Gabriel SE, Randell SH, Harfe BD, Boucher RC, et al. Transmembrane protein 16A (TMEM16A) is a  $\text{Ca}^{2+}$ -regulated  $\text{Cl}^-$  secretory channel in mouse airways. *J Biol Chem* 2009;**284**:14875–80.
- Davis AJ, Forrest AS, Jepps TA, Valencik ML, Wiwchar M, Singer CA, et al. Expression profile and protein translation of TMEM16A in murine smooth muscle. *Am J Physiol Cell Physiol* 2010;**299**:948–59.
- Caputo A, Caci E, Ferrera L, Pedemonte N, Barsanti C, Sondo E, et al. TMEM16A, a membrane protein associated with calcium-dependent chloride channel activity. *Science* 2008;**322**:590–4.
- Schroeder BC, Cheng T, Jan YN, Jan LY. Expression cloning of TMEM16A as a calcium-activated chloride channel subunit. *Cell* 2008;**134**:1019–29.
- Yang YD, Cho HW, Koo JY, Tak MH, Cho YY, Shim WS, et al. TMEM16A confers receptor-activated calcium-dependent chloride conductance. *Nature* 2008;**455**:1210–36.
- Ferrera L, Caputo A, Galiotta LJV. TMEM16A protein: A new identity for  $\text{Ca}^{2+}$ -dependent  $\text{Cl}^-$  channels. *Physiology* 2010;**25**:357–63.
- Benedetto R, Cabrita I, Schreiber R, Kunzelmann K. TMEM16A is indispensable for basal mucus secretion in airways and intestine. *FASEB J* 2019;**33**:4502–12.
- Truong EC, Phuan PW, Reggi AL, Ferrera L, Galiotta LJV, Levy SE, et al. Substituted 2-acylaminoalkylthiophene-3-carboxylic acid arylamides as inhibitors of the calcium-activated chloride channel transmembrane protein 16a (TMEM16A). *J Med Chem* 2017;**60**:4626–35.
- Liu BY, Linley JE, Du XN, Zhang X, Ooi L, Zhang HL, et al. The acute nociceptive signals induced by bradykinin in rat sensory neurons are mediated by inhibition of M-type  $\text{K}^+$  channels and activation of  $\text{Ca}^{2+}$ -activated  $\text{Cl}^-$  channels. *J Clin Invest* 2010;**120**:1240–52.
- Miner K, Labitzke K, Liu B, Wang P, Henckels K, Gaida K, et al. Drug repurposing: The anthelmintics niclosamide and nitazoxanide are potent TMEM16A antagonists that fully bronchodilate airways. *Front Pharmacol* 2019;**10**:51–80.
- Espinosa I, Lee CH, Kim MK, Rouse BT, Subramanian S, Montgomery K, et al. A novel monoclonal antibody against DOG1 is a sensitive and specific marker for gastrointestinal stromal tumors. *Am J Surg Pathol* 2008;**32**:210–8.
- Duvvuri U, Shiwarski DJ, Xiao D, Bertrand C, Huang X, Edinger RS, et al. TMEM16A induces MAPK and contributes directly to tumorigenesis and cancer progression. *Cancer Res* 2012;**72**:3270–81.
- Bill A, Hall ML, Borawski J, Hodgson C, Jenkins J, Piechon P, et al. Small molecule-facilitated degradation of ANO1 protein. *J Biol Chem* 2014;**289**:11029–41.
- Garcia G, Martinez-Rojas VA, Oviedo N, Murbartian J. Blockade of Anoctamin-1 in injured and uninjured nerves reduces neuropathic pain. *Brain Res* 2018;**1696**:38–48.
- Pineda-Farias JB, Barragan-Iglesias P, Loeza-Alcocer E, Torres-Lopez JE, Rocha-Gonzalez HI, Perez-Severiano F, et al. Role of anoctamin-1 and bestrophin-1 in spinal nerve ligation-induced neuropathic pain in rats. *Mol Pain* 2015;**11**:41–56.
- Lee B, Cho H, Jung J, Yang YD, Yang DJ, Oh U. Anoctamin 1 contributes to inflammatory and nerve-injury induced hypersensitivity. *Mol Pain* 2014;**10**:5–15.
- Deba F, Bessac BF. Anoctamin-1  $\text{Cl}^-$  channels in nociception: activation by an *N*-aroylaminothiazole and capsaicin and inhibition by T16A<sub>inh</sub>-A01. *Mol Pain* 2015;**11**:55–63.
- Garcia G, Martinez-Rojas VA, Rocha-Gonzalez HI, Granados-Soto V, Murbartian J. Evidence for the participation of  $\text{Ca}^{2+}$ -activated chloride channels in formalin-induced acute and chronic nociception. *Brain Res* 2014;**1579**:35–44.
- Takayama Y, Derouiche S, Maruyama K, Tominaga M. Emerging perspectives on pain management by modulation of TRP channels and ANO1. *Int J Mol Sci* 2019;**20**:124–36.
- Takayama Y, Uta D, Furue H, Tominaga M. Pain-enhancing mechanism through interaction between TRPV1 and anoctamin 1 in sensory neurons. *Proc Natl Acad Sci U S A* 2015;**112**:5213–8.
- Cho H, Yang YD, Lee J, Lee B, Kim T, Jang Y, et al. The calcium-activated chloride channel Anoctamin 1 acts as a heat sensor in nociceptive neurons. *Nat Neurosci* 2012;**15**:1015–21.
- De La Fuente R, Namkung W, Mills A, Verkman AS. Small-molecule screen identifies inhibitors of a human intestinal calcium-activated chloride channel. *Mol Pharmacol* 2008;**73**:758–68.
- Namkung W, Phuan PW, Verkman AS. TMEM16A inhibitors reveal TMEM16A as a minor component of calcium-activated chloride channel conductance in airway and intestinal epithelial cells. *J Biol Chem* 2011;**286**:2365–74.
- Oh SJ, Hwang SJ, Jung J, Yu K, Kim J, Choi JY, et al. MONNA, a potent and selective blocker for transmembrane protein with unknown function 16/Anoctamin-1. *Mol Pharmacol* 2013;**84**:726–35.
- Seo Y, Lee HK, Park J, Jeon DK, Jo S, Jo M, et al. Ani9, a novel potent small-molecule ANO1 inhibitor with negligible effect on ANO2. *PLoS One* 2016;**11**:81–9.
- Namkung W, Thiagarajah JR, Phuan PW, Verkman AS. Inhibition of  $\text{Ca}^{2+}$ -activated  $\text{Cl}^-$  channels by gallotannins as a possible molecular basis for health benefits of red wine and green tea. *FASEB J* 2010;**24**:4178–86.
- Ji Q, Guo S, Wang X, Pang C, Zhan Y, Chen Y, et al. Recent advances in TMEM16A: structure, function, and disease. *J Cell Physiol* 2019;**234**:7856–73.

30. Seo Y, Ryu K, Park J, Jeon DK, Jo S, Lee HK, et al. Inhibition of ANO1 by luteolin and its cytotoxicity in human prostate cancer PC-3 cells. *PLoS One* 2017;**12**:534–55.
31. Chai R, Chen Y, Yuan H, Wang X, Guo S, Qi J, et al. Identification of resveratrol, an herbal compound, as an activator of the calcium-activated chloride channel, TMEM16A. *J Membr Biol* 2017;**250**:483–92.
32. Nishimura K, Yamamura H, Imaizumi Y. Functional expression of Ca<sup>2+</sup>-activated Cl<sup>-</sup> (TMEM16B) channel in rat pineal glands. *J Pharmacol Sci* 2014;**124**:1223–35.
33. Abaee MS, Hadizadeh A, Mojtahedi MM, Halvagar MR. Exploring the scope of the Gewald reaction: Expansion to a four-component process. *Tetrahedron Lett* 2017;**58**:1408–12.
34. Zhang Y, Zhang ZS, Xiao SH, Tien J, Le S, Le T, et al. Inferior olivary TMEM16B mediates cerebellar motor learning. *Neuron* 2017;**95**:1103–14.
35. Yamamura H, Nishimura K, Hagihara Y, Suzuki Y, Imaizumi Y. TMEM16A and TMEM16B channel proteins generate Ca<sup>2+</sup>-activated Cl<sup>-</sup> current and regulate melatonin secretion in rat pineal glands. *J Biol Chem* 2018;**293**:995–1006.
36. Paulino C, Neldner Y, Lam AK, Kalienkova V, Brunner JD, Schenck S, et al. Structural basis for anion conduction in the calcium-activated chloride channel TMEM16A. *Elife* 2017;**6**:65–75.
37. Bill A, Popa MO, van Diepen MT, Gutierrez A, Lilley S, Velkova M, et al. Variomics screen identifies the re-entrant loop of the calcium-activated chloride channel ANO1 that facilitates channel activation. *J Biol Chem* 2015;**290**:889–903.
38. Brunner JD, Lim NK, Schenck S, Duerst A, Dutzler R. X-ray structure of a calcium-activated TMEM16 lipid scramblase. *Nature* 2014;**516**:207–15.
39. Dang S, Feng S, Tien J, Peters CJ, Bulkley D, Lolicato M, et al. Cryo-EM structures of the TMEM16A calcium-activated chloride channel. *Nature* 2017;**552**:426–9.
40. Paulino C, Kalienkova V, Lam AKM, Neldner Y, Dutzler R. Activation mechanism of the calcium-activated chloride channel TMEM16A revealed by cryo-EM. *Nature* 2017;**552**:421–5.
41. Seo Y, Kim J, Chang J, Kim SS, Namkung W, Kim I. Synthesis and biological evaluation of novel Ani9 derivatives as potent and selective ANO1 inhibitors. *Eur J Med Chem* 2018;**160**:245–55.
42. Okuda K, Sakurada C, Takahashi M, Yamada T, Sakurada T. Characterization of nociceptive responses and spinal releases of nitric oxide metabolites and glutamate evoked by different concentrations of formalin in rats. *Pain* 2001;**92**:107–15.
43. Chaplan SR, Bach FW, Pogrel JW, Chung JM, Yaksh TL. Quantitative assessment of tactile allodynia in the rat paw. *J Neurosci Methods* 1994;**53**:55–63.
44. Bennett GJ, Xie YK. A peripheral mononeuropathy in rat that produces disorders of pain sensation like those seen in man. *Pain* 1988;**33**:87–107.
45. Hargreaves K, Dubner R, Brown F, Flores C, Joris J. A new and sensitive method for measuring thermal nociception in cutaneous hyperalgesia. *Pain* 1988;**32**:77–88.
46. Masocha W, Kombian SB, Edafiogho IO. Evaluation of the anti-nociceptive activities of enaminone compounds on the formalin and hot plate tests in mice. *Sci Rep* 2016;**6**:53–66.